Eidgenössische Technische Hochschule Zürich

Ecole polytechnique fédérale de Zurich
Politecnico federale di Zurigo
Swiss Federal Institute of Technology Zurich

Arbitrarily high order accurate entropy stable essentially non-oscillatory schemes for systems of conservation laws

U.S. Fjordholm, S. Mishra and E. Tadmor*

Research Report No. 2011-39
June 2011

Seminar für Angewandte Mathematik
Eidgenössische Technische Hochschule
CH-8092 Zürich
Switzerland

*Dept. of Mathematics, University of Maryland, MD 20742-4015, USA

ARBITRARILY HIGH ORDER ACCURATE ENTROPY STABLE ESSENTIALLY NON-OSCILLATORY SCHEMES FOR SYSTEMS OF CONSERVATION LAWS.

U. S. FJORDHOLM, S. MISHRA, AND E. TADMOR

Abstract. We design arbitrarily high-order accurate entropy stable schemes for systems of conservation laws. The schemes, termed *TeCNO schemes*, are based on two main ingredients: (i) high-order accurate *entropy conservative* fluxes, and (ii) suitable numerical diffusion operators involving ENO reconstructed cell-interface values of scaled entropy variables. Numerical experiments in one and two space dimensions are presented to illustrate the robust numerical performance of the TeCNO schemes.

1. Introduction

Systems of conservation laws are ubiquitous in science and engineering. They encompass applications in oceanography (shallow water equations), aerodynamics (Euler equations), plasma physics (MHD equations) and structural mechanics (non-linear elasticity). In one space dimension, these PDEs are of the form

$$\begin{aligned} \mathbf{u}_t + \mathbf{f}(\mathbf{u})_x = 0 \qquad & \forall\ (x,t) \in \mathbb{R}\times\mathbb{R}_+, \\ \mathbf{u}(x,0) = \mathbf{u}_0(x) \qquad & \forall\ x \in \mathbb{R}. \end{aligned} \tag{1.1}$$

$\mathbf{u} : \mathbb{R}\times\mathbb{R}_+ \mapsto \mathbb{R}^m$ is the vector of unknowns and $\mathbf{f}$ is the (non-linear) flux vector. It is well-known that solutions of (1.1) contain discontinuities in the form of shock waves, even for smooth initial data [6]. Hence, solutions of (1.1) are sought in a weak sense. A function $\mathbf{u} \in L^\infty(\mathbb{R}\times\mathbb{R}_+)$ is a *weak solution* of (1.1) if

$$\int_{\mathbb{R}}\int_{\mathbb{R}_+} \mathbf{u}\varphi_t + \mathbf{f}(\mathbf{u})\varphi_x \ dxdt + \int_{\mathbb{R}} \mathbf{u}(x,0)\varphi(x,0)\ dx = 0 \tag{1.2}$$

for all compactly supported smooth test functions $\varphi \in C_c^1(\mathbb{R}\times\mathbb{R}_+)$.

Weak solutions might not be unique and need to be supplemented with extra admissibility criteria, termed *entropy conditions*, in order to single out a physically relevant solution [6]. Assume that there exists a convex function $E : \mathbb{R}^m \to \mathbb{R}$ and a function $Q : \mathbb{R}^m \to \mathbb{R}$ such that $\partial_{\mathbf{u}} Q(\mathbf{u}) = \mathbf{v}^\top \partial_{\mathbf{u}} \mathbf{f}(\mathbf{u})$, where $\mathbf{v} := \partial_{\mathbf{u}} E(\mathbf{u})$. The functions E, Q and $\mathbf{v}$ are termed the entropy function, entropy flux function and entropy variables, respectively. Multiplying (1.1) by the entropy variables $\mathbf{v}^\top$ shows that *smooth* solutions of (1.1) satisfy the entropy identity

$$E(\mathbf{u})_t + Q(\mathbf{u})_x = 0. \tag{1.3}$$

However, the solutions of (1.1) are not smooth in general and the entropy has to be dissipated at shocks. This translates into the entropy inequality

$$E(\mathbf{u})_t + Q(\mathbf{u})_x \leq 0 \tag{1.4}$$

(in the sense of distributions). Formally, integrating (1.4) in space and asserting a periodic or no-inflow boundary, we obtain the bound

$$\frac{d}{dt}\int_{\mathbb{R}} E(\mathbf{u})dx \leq 0 \quad \Rightarrow \quad \int_{\mathbb{R}} E\left(\mathbf{u}(x,T)\right) dx \leq \int_{\mathbb{R}} E(\mathbf{u}_0(x))dx \tag{1.5}$$

for all $T > 0$. As E is convex, the above entropy bound can be converted into an a priori estimate on the solution of (1.1) in suitable L^p spaces [6].

Date: June 7, 2011.

1991 *Mathematics Subject Classification.* 65M06,35L65.

The research of ET was supported by grants from National Science Foundation DMS#10-08397, and the Office of Naval Research ONR#N000140910385.

1.1. **Numerical schemes.** The design of efficient numerical schemes for the approximation of hyperbolic conservation laws has undergone extensive development. Finite volume (conservative finite difference) methods are among the most popular discretization frameworks. We consider a uniform Cartesian mesh $\{x_i\}_{i\in\mathbb{Z}}$ in $\mathbb{R}$ with mesh size $x_{i+1} - x_i = \Delta x$. The midpoint values are defined as $x_{i+1/2} := \frac{x_i+x_{i+1}}{2}$ and the domain is partitioned into intervals $I_i = [x_{i-1/2}, x_{i+1/2}]$. The conservative finite difference (finite volume) method updates point values (cell averages in I_i) of the solution $\mathbf{u}$, and has the general form

$$\frac{d}{dt}\mathbf{u}_i(t) = -\frac{1}{\Delta x}\left(\mathbf{F}_{i+1/2}(t) - \mathbf{F}_{i-1/2}(t)\right), \tag{1.6}$$

where the numerical flux $\mathbf{F}_{i+1/2} = \mathbf{F}(\mathbf{u}_i(t), \mathbf{u}_{i+1}(t))$ is computed from an (approximate) solution of the Riemann problem at the interface $x_{i+1/2}$ [19].

Second order spatial accuracy can be obtained with non-oscillatory TVD methods [17], and even higher order of accuracy can be obtained with ENO [12] and WENO [24] piecewise polynomial reconstructions. An alternative approach to a high order of spatial accuracy is the *Discontinuous Galerkin*(DG) method of [3]. The DG method requires TVB limiters to suppress oscillations near discontinuities. Time integration for the semi-discrete scheme (1.6) is performed with strong stability preserving Runge-Kutta methods [10] or with ADER schemes [32].

1.2. **Accuracy and stability.** For scalar conservation laws in one space dimension, monotone (first-order) schemes were shown to be TVD in [11] and consistent with any entropy condition in [5]. Hence, these schemes converge to the entropy solution. *E-schemes* for scalar conservation laws that preserve a discrete version of the entropy inequality (1.4) were designed by Tadmor [27] and Osher [22]. Convergence results for monotone schemes for multi-dimensional scalar conservation laws were obtained in [2].

Second-order accurate limiter-based schemes for scalar conservation laws were shown to be stable in BV in [26]. Second-order entropy stable schemes for scalar conservation laws were presented in [23]. Stability results in BV for second-order and third-order accurate central schemes in the scalar case were shown in [21] and [20] respectively.

Very few stability results exist for schemes that approximate scalar conservation laws with even higher (≥ 3) order of accuracy. We mention [15] in which WENO schemes were shown to converge for smooth solutions of scalar conservation laws. This result is quite limited as solutions of the conservation law (1.1) have discontinuities. Convergence results for a streamline diffusion finite element method were shown in [16]. The arbitrary order Discontinuous Galerkin (DG) methods were shown in [4] to satisfy a global entropy estimate, i.e, a discrete version of (1.5) for scalar conservation laws. Note that these methods might not satisfy a local version of the discrete entropy inequality (1.4). DG methods must be limited by a TVD or TVB limiter in order to obtain BV bounds. Entropy stable *limited* DG methods are not currently available.

Convergence results for numerical schemes (even first-order schemes) approximating non-linear systems of conservation laws are difficult to obtain, as a global well-posedness theory for such equations is not currently available. It is reasonable to require that numerical schemes are entropy stable, i.e, satisfy a discrete version of the entropy inequality (1.4). In particular, such a scheme satisfies a discrete form of the entropy bound (1.5) and will be stable in a suitable L^p space. No entropy stability results for high-order numerical schemes for approximating systems of conservation laws, based on the TVD, ENO, WENO and DG procedures, are available. Entropy stable streamline diffusion finite element methods were proposed in [13].

1.3. **Scope and outline of the paper.** In view of the above discussion, it is fair to claim that none of the currently available high and very high-order schemes for systems of conservation laws have been rigorously shown to be stable. Given this background, we present a class of schemes in this paper that are

(i) (Formally) arbitrarily order accurate;
(ii) Entropy stable for *any* system of conservation laws;
(iii) Essentially non-oscillatory around discontinuities;
(iv) Convergent for linear symmetrizable systems;
(v) Computationally efficient.

We recall that entropy stability automatically provides an a priori estimate on the scheme in $L^p(\mathbb{R})$. Our schemes do not contain any tuning parameters.

Our schemes are based on the following two ingredients:

Entropy conservative fluxes: The first step in the construction of entropy stable schemes is to use entropy conservative fluxes, introduced by Tadmor in [28, 29]. More recent developments on entropy conservative fluxes are described in [7, 8, 14, 30, 31]. These papers construct second-order accurate entropy conservative schemes. Even higher order accurate entropy conservative fluxes were proposed in [18, 29]. We utilize the procedure of [18] along with explicit formulas obtained in [7, 14] to construct computationally efficient, arbitrarily high-order accurate entropy conservative fluxes.

Numerical diffusion operators: Following [7, 29], we add numerical diffusion in terms of *entropy variables* to a entropy conservative scheme to obtain an entropy stable scheme. Arbitrary order of accuracy is obtained by using piecewise polynomial reconstructions. We rely on a subtle non-oscillatory property, the so-called *sign property* of the ENO reconstruction procedure, to prove entropy stability. The sign property of the ENO reconstruction procedure was shown in a recent paper [9].

We term this combination of The Entropy Conservative and ENO reconstruction procedures as *TeCNO* schemes and show that they are entropy stable while having a (formally) arbitrarily high order of accuracy. The TeCNO schemes are easily extended to several space dimensions.

The rest of the paper is organized as follows: in Section 2, we describe the procedure of [18] and the two-point entropy conservative fluxes of [7, 14], and construct high-order accurate entropy conservative schemes. The entropy stable numerical diffusion operators of arbitrarily high order of accuracy are proposed in Section 3. The TeCNO schemes are presented in Section 4. Numerical experiments are presented in Section 5 and the extension to several space dimensions is provided in Section 6.

2. Entropy conservative fluxes

In this section we review theory on entropy conservative schemes. These are schemes whose computed solutions satisfy a discrete entropy equality

$$\frac{d}{dt}E(\mathbf{u}_i(t)) = -\frac{1}{\Delta x}\left(\widetilde{Q}_{i+1/2} - \widetilde{Q}_{i-1/2}\right) \tag{2.1}$$

for some *numerical entropy flux* $\widetilde{Q}_{i+1/2}$ consistent with Q. We introduce the following notation:

$$[\![a]\!]_{i+1/2} = a_{i+1} - a_i, \qquad \overline{a}_{i+1/2} = \frac{1}{2}(a_i + a_{i+1}).$$

We will also use *entropy potential* $\psi(\mathbf{u}) := \mathbf{v}(\mathbf{u})^\top \mathbf{f}(\mathbf{u}) - Q(\mathbf{u})$.

Theorem 2.1 (Tadmor [28])**.** *Assume that a consistent numerical flux* $\widetilde{\mathbf{F}}_{i+1/2}$ *satisfies*

$$[\![\mathbf{v}]\!]^\top_{i+1/2}\widetilde{\mathbf{F}}_{i+1/2} = [\![\psi]\!]_{i+1/2}. \tag{2.2}$$

Then the scheme with numerical flux $\widetilde{\mathbf{F}}_{i+1/2}$ *is second-order accurate and entropy conservative – solutions computed by the scheme satisfy the discrete entropy equality* (2.1) *with numerical entropy flux*

$$\widetilde{Q}_{i+1/2} = \overline{\mathbf{v}}^\top_{i+1/2}\widetilde{\mathbf{F}}_{i+1/2} - \overline{\psi}_{i+1/2}. \tag{2.3}$$

We note that the condition (2.2) provides a single algebraic equation for m unknowns. In general, it is not clear whether a solution of (2.2) exists. Furthermore, the solutions of (2.2) will not be unique except in the case of scalar equations ($m = 1$).

In [28], Tadmor showed the existence of a solution for the equation (2.2) for a general system of conservation laws by the following procedure: for $\xi \in [-1/2, 1/2]$, define the following straight line in phase space:

$$\mathbf{v}_{i+1/2}(\xi) = \frac{1}{2}(\mathbf{v}_i + \mathbf{v}_{i+1}) + \xi(\mathbf{v}_{i+1} - \mathbf{v}_i). \tag{2.4}$$

The numerical flux is then defined as the path integral

$$\widetilde{\mathbf{F}}_{i+1/2} = \int_{-1/2}^{1/2} \mathbf{f}(\mathbf{v}_{i+1/2}(\xi))d\xi. \tag{2.5}$$

However, it may be very hard to evaluate the path integral (2.5) except in very special cases [7].

An explicit solution of (2.2) was devised in [29]. Take any orthogonal eigensystem r_k, l_k for $k = 1, 2, \ldots, m$. At an interface $x_{i+1/2}$, we have the two adjacent entropy variable vectors $\mathbf{v}_i$ and $\mathbf{v}_{i+1}$. Define

$$\begin{aligned} \mathbf{v}^0 &= \mathbf{v}_i \\ \mathbf{v}^k &= \mathbf{v}^{k-1} + \left([\![\mathbf{v}]\!]_{i+1/2}^\top l_k \right) r_k \qquad (k = 1, \ldots, m-1) \\ \mathbf{v}^m &= \mathbf{v}_{i+1}. \end{aligned}$$

We are replacing the straight line joining the two adjacent states in the flux (2.5) by a piecewise linear path along basis vectors. The resulting entropy conservative flux is given by

$$\widetilde{\mathbf{F}}_{i+1/2} = \sum_{k=1}^{n} \frac{\psi(\mathbf{v}^k) - \psi(\mathbf{v}^{k-1})}{[\![\mathbf{v}]\!]_{i+1/2}^\top l_k} l_k \tag{2.6}$$

This construction is very general and works for any system of conservation laws. However, the computation of (2.6) may be both expensive and numerically unstable [7]. Therefore, we follow a different approach and find explicit algebraic solutions of (2.2) for specific systems.

2.1. **Examples.** We consider specific hyperbolic conservation laws and describe explicit and computationally inexpensive entropy conservative fluxes satisfying (2.2).

2.1.1. *Scalar conservation laws.* Consider the scalar version of (1.1) and denote $u = \mathbf{u}$, $f = \mathbf{f}$. Any convex function E can serve as an entropy function. Let v and ψ be the corresponding entropy variable and potential, respectively. It is straightforward to compute the *unique* entropy conservative flux $\widetilde{F}$ in this case as

$$\widetilde{F}(u_i, u_{i+1}) = \begin{cases} \frac{\psi_{i+1} - \psi_i}{v_{i+1} - v_i} & \text{if } u_i \neq u_{i+1} \\ f(u_i) & \text{otherwise.} \end{cases} \tag{2.7}$$

2.1.2. *Linear symmetrizable systems.* Let $\mathbf{f}(\mathbf{u}) = \mathbf{A}\mathbf{u}$ with $\mathbf{A}$ being a (constant) $m \times m$ matrix. Assume that there exists a symmetric positive definite matrix $\mathbf{S}$ such that $\mathbf{SA}$ is symmetric. Then

$$E(\mathbf{u}) = \frac{1}{2}\mathbf{u}^\top \mathbf{S}\mathbf{u}, \qquad Q(\mathbf{u}) = \frac{1}{2}\mathbf{u}^\top \mathbf{S}\mathbf{A}\mathbf{u} \tag{2.8}$$

constitute an entropy-entropy flux pair for the linear system. The entropy variables and -potential are given by

$$\mathbf{v} = \mathbf{S}\mathbf{u}, \qquad \psi(\mathbf{u}) = \frac{1}{2}\mathbf{u}^\top \mathbf{S}\mathbf{A}\mathbf{u}$$

Inserting into (2.5), one easily finds the entropy conservative flux

$$\widetilde{\mathbf{F}}_{i+1/2} = \frac{1}{2}\left(\mathbf{A}\mathbf{u}_i + \mathbf{A}\mathbf{u}_{i+1}\right). \tag{2.9}$$

2.1.3. *Shallow water equations.* The shallow water equations model a body of water under the influence of gravity, and has conservative variables and flux

$$\mathbf{u} = \begin{bmatrix} h \\ hu \end{bmatrix}, \qquad \mathbf{f}(\mathbf{u}) = \begin{bmatrix} hu \\ hu^2 + \frac{1}{2}gh^2 \end{bmatrix}. \tag{2.10}$$

Here, h and u are the depth and velocity of the water, respectively. The (constant) acceleration due to gravity is denoted by g. The entropy in this case is the total energy:

$$E(\mathbf{u}) = \frac{hu^2 + gh^2}{2}, \qquad Q(\mathbf{u}) = \frac{hu^3}{2} + guh^2. \tag{2.11}$$

The corresponding entropy variables and potential are given by

$$\mathbf{v} = \begin{bmatrix} gh - \frac{u^2}{2} \\ u \end{bmatrix}, \qquad \psi(\mathbf{u}) = \frac{1}{2}guh^2. \tag{2.12}$$

An explicit solution of (2.2) for the shallow water equations was proposed in the recent paper [7]:

$$\widetilde{\mathbf{F}}_{i+1/2} = \begin{bmatrix} \overline{h}_{i+1/2}\overline{u}_{i+1/2} \\ \overline{h}_{i+1/2}(\overline{u}_{i+1/2})^2 + \frac{g}{2}\overline{h^2}_{i+1/2} \end{bmatrix}. \tag{2.13}$$

The above flux is clearly consistent, very simple to implement and computationally inexpensive.

2.1.4. *Euler equations.* Let

$$\mathbf{u} = \begin{bmatrix} \rho \\ \rho u \\ \mathcal{E} \end{bmatrix}, \qquad \mathbf{f}(\mathbf{u}) = \begin{bmatrix} \rho u \\ \rho u^2 + p \\ (\mathcal{E}+p)u \end{bmatrix}. \tag{2.14}$$

Here, ρ, u and p are the density, velocity and pressure of the gas. The total energy $\mathcal{E}$ is related to other variables by the equation of state:

$$\mathcal{E} = \frac{p}{\gamma - 1} + \frac{1}{2}\rho u^2, \tag{2.15}$$

with γ being the gas constant. Let $s = \log(p) - \gamma \log(\rho)$ be the thermodynamic entropy. An entropy-entropy flux pair for the Euler equations is

$$E = \frac{-\rho s}{\gamma - 1}, \qquad Q = \frac{-\rho u s}{\gamma - 1}. \tag{2.16}$$

The corresponding entropy variables and -potential are

$$\mathbf{v} = \begin{bmatrix} \frac{\gamma - s}{\gamma - 1} - \frac{\rho u^2}{2p} \\ \frac{\rho u}{p} \\ -\frac{\rho}{p} \end{bmatrix}, \qquad \psi(\mathbf{u}) = \rho u. \tag{2.17}$$

In a recent paper [14], Ismail and Roe have constructed an explicit solution of (2.2) for the Euler equations. Defining the parameter vectors $\mathbf{z}$ as

$$\mathbf{z} = \begin{bmatrix} z^1 \\ z^2 \\ z^3 \end{bmatrix} = \sqrt{\frac{\rho}{p}} \begin{bmatrix} 1 \\ u \\ p \end{bmatrix}, \tag{2.18}$$

the entropy conservative flux of [14] is $\widetilde{\mathbf{F}}_{i+1/2} = \begin{bmatrix} \widetilde{\mathbf{F}}^1_{i+1/2} & \widetilde{\mathbf{F}}^2_{i+1/2} & \widetilde{\mathbf{F}}^3_{i+1/2} \end{bmatrix}^\top$ with

$$\begin{aligned} \widetilde{\mathbf{F}}^1_{i+1/2} &= \overline{z^2}_{i+1/2} \left(z^3\right)^{\ln}_{i+1/2} \\ \widetilde{\mathbf{F}}^2_{i+1/2} &= \frac{\overline{z^3}_{i+1/2}}{\overline{z^1}_{i+1/2}} + \frac{\overline{z^2}_{i+1/2}}{\overline{z^1}_{i+1/2}} \widetilde{\mathbf{F}}^1_{i+1/2} \\ \widetilde{\mathbf{F}}^3_{i+1/2} &= \frac{1}{2} \frac{\overline{z^2}_{i+1/2}}{\overline{z^1}_{i+1/2}} \left(\frac{\gamma+1}{\gamma-1} \frac{\left(z^3\right)^{\ln}_{i+1/2}}{\left(z^1\right)^{\ln}_{i+1/2}} + \widetilde{\mathbf{F}}^2_{i+1/2} \right) \end{aligned} \tag{2.19}$$

Here, $a^{\ln}$ is the logarithmic mean, defined as

$$a^{\ln}_{i+1/2} = \frac{[\![a]\!]_{i+1/2}}{[\![\log(a)]\!]_{i+1/2}}.$$

The above examples show that we can obtain explicit and computationally inexpensive expressions of entropy conservative fluxes for a large class of systems. In case such explicit formulas are not available, we can use (2.6) to compute the two point entropy conservative flux.

2.2. **High-order entropy conservative fluxes.** The entropy conservative fluxes defined above are only second-order accurate. However, following the procedure of LeFloch, Mercier and Rohde [18], we can use these fluxes as building blocks to obtain $2p$-th order accurate entropy conservative fluxes for *any* $p \in \mathbb{N}$. These consist of linear combinations of second-order accurate entropy conservative fluxes $\widetilde{\mathbf{F}}$, and have the form

$$\widetilde{\mathbf{F}}^{2p}_{i+1/2} = \sum_{r=1}^{p} \alpha^p_r \sum_{s=0}^{r-1} \widetilde{\mathbf{F}}(\mathbf{u}_{i-s}, \mathbf{u}_{i-s+r}). \tag{2.20}$$

Theorem 2.2. [18, Theorem 4.4] *For $p \in \mathbb{N}$, assume that $\alpha^p_1, \ldots, \alpha^p_p$ solve the p linear equations*

$$2\sum_{r=1}^{p} r\alpha^p_r = 1, \qquad \sum_{i=1}^{p} i^{2s-1}\alpha^p_r = 0 \quad (s = 2, \ldots, p),$$

and define $\widetilde{\mathbf{F}}^{2p}$ by (2.20)*. Then the finite difference scheme with flux $\widetilde{\mathbf{F}}^{2p}$ is*

(i) $2p$-th order accurate, in the sense that for sufficiently smooth solutions $\mathbf{u}$ *we have*

$$\frac{1}{\Delta x}\left(\widetilde{\mathbf{F}}^{2p}\left(\mathbf{u}_{i-p+1},\ldots,\mathbf{u}_{i+p}\right)-\widetilde{\mathbf{F}}^{2p}\left(\mathbf{u}_{i-p},\ldots,\mathbf{u}_{i+p-1}\right)\right)=\partial_x\mathbf{f}(\mathbf{u}_i)+\mathcal{O}\left(\Delta x^{2p}\right).$$

(ii) entropy conservative – it satisfies the discrete entropy identity

$$\frac{d}{dt}E(\mathbf{u}_i(t))+\frac{1}{\Delta x}\left(\widetilde{Q}^{2p}_{i+1/2}-\widetilde{Q}^{2p}_{i-1/2}\right)=0$$

where

$$\widetilde{Q}^{2p}_{i+1/2}=\sum_{r=1}^{p}\alpha_r^p\sum_{s=0}^{r-1}\widetilde{Q}(\mathbf{u}_{i-s},\mathbf{u}_{i-s+r}) \tag{2.21}$$

As an example, the fourth-order ($p=2$) version of the entropy conservative flux (2.20) is

$$\widetilde{\mathbf{F}}^4_{i+1/2}=\frac{4}{3}\widetilde{\mathbf{F}}(\mathbf{u}_i,\mathbf{u}_{i+1})-\frac{1}{6}\left(\widetilde{\mathbf{F}}(\mathbf{u}_{i-1},\mathbf{u}_{i+1})+\widetilde{\mathbf{F}}(\mathbf{u}_i,\mathbf{u}_{i+2})\right) \tag{2.22}$$

and the sixth-order ($p=3$) version

$$\begin{aligned}\widetilde{\mathbf{F}}^6_{i+1/2}=&\frac{3}{2}\widetilde{\mathbf{F}}(\mathbf{u}_i,\mathbf{u}_{i+1})-\frac{3}{10}\left(\widetilde{\mathbf{F}}(\mathbf{u}_{i-1},\mathbf{u}_{i+1})+\widetilde{\mathbf{F}}(\mathbf{u}_i,\mathbf{u}_{i+2})\right)\\&+\frac{1}{30}\left(\widetilde{\mathbf{F}}(\mathbf{u}_{i-2},\mathbf{u}_{i+1})+\widetilde{\mathbf{F}}(\mathbf{u}_{i-1},\mathbf{u}_{i+2})+\widetilde{\mathbf{F}}(\mathbf{u}_i,\mathbf{u}_{i+3})\right).\end{aligned} \tag{2.23}$$

Remark 2.3. Since the high-order entropy conservative fluxes (2.20) are based on linear combinations of two-point second order fluxes $\widetilde{\mathbf{F}}$, they are computationally tractable only if computationally inexpensive two-point fluxes like those described in the previous section are available.

3. Numerical Diffusion operators

The entropy of solutions of hyperbolic conservation laws is only conserved if the solution is smooth. However, the solutions develop discontinuities where entropy is *dissipated*, which is reflected in the entropy inequality (1.4). The entropy conservative schemes described in the previous section will produce high-frequency oscillations near shocks (see [7] for numerical examples). Consequently, we need to add some dissipative mechanism to ensure that entropy is dissipated. This is achieved by designing *entropy stable schemes* – schemes whose computed solutions satisfy a discrete entropy inequality

$$\frac{d}{dt}E(\mathbf{u}_i)+\frac{1}{\Delta x}\left(\widehat{Q}_{i+1/2}-\widehat{Q}_{i-1/2}\right)\leq 0 \tag{3.1}$$

for some numerical entropy flux function $\widehat{Q}_{i+1/2}$ consistent with Q.

3.1. First-order numerical diffusion operator.

We begin with the second-order entropy conservative flux $\widetilde{\mathbf{F}}$ (2.2) and add a numerical diffusion term to define

$$\mathbf{F}_{i+1/2}=\widetilde{\mathbf{F}}_{i+1/2}-\frac{1}{2}\mathbf{D}_{i+1/2}[\![\mathbf{v}]\!]_{i+1/2}. \tag{3.2}$$

Here, $\mathbf{D}$ is any symmetric positive definite matrix.

Lemma 3.1 (Tadmor [28])**.** *The scheme with flux* (3.2) *is entropy stable – its solutions satisfy*

$$\frac{d}{dt}E(\mathbf{u}_i)+\frac{1}{\Delta x}\left(\widehat{Q}_{i+1/2}-\widehat{Q}_{i-1/2}\right)=-\frac{1}{4\Delta x}\left([\![\mathbf{v}]\!]^\top_{i+1/2}\mathbf{D}_{i+1/2}[\![\mathbf{v}]\!]_{i+1/2}+[\![\mathbf{v}]\!]^\top_{i-1/2}\mathbf{D}_{i-1/2}[\![\mathbf{v}]\!]_{i-1/2}\right)\leq 0, \tag{3.3}$$

where

$$\widehat{Q}_{i+1/2}=\widetilde{Q}_{i+1/2}+\frac{1}{2}\overline{\mathbf{v}}^\top_{i+1/2}\mathbf{D}_{i+1/2}[\![\mathbf{v}]\!]_{i+1/2}$$

and $\widetilde{Q}_{i+1/2}$ *is the numerical entropy flux function of the flux* $\widetilde{\mathbf{F}}_{i+1/2}$*.*

As a corollary, we can sum (3.3) over all i to obtain the entropy dissipation estimate

$$\frac{d}{dt}\sum_i E(\mathbf{u}_i)=-\frac{1}{2\Delta x}\sum_i[\![\mathbf{v}]\!]^\top_{i+1/2}\mathbf{D}_{i+1/2}[\![\mathbf{v}]\!]_{i+1/2}\leq 0$$

Although the above lemma holds for any symmetric positive definite $\mathbf{D}_{i+1/2}$, we will use diffusion matrices of the form

$$\mathbf{D}_{i+1/2} = R\Lambda R^\top. \tag{3.4}$$

Here, R is the matrix of eigenvectors of the flux Jacobian $\partial_{\mathbf{u}}\mathbf{f}$ and Λ is a positive diagonal matrix that depends on the eigenvalues of the flux Jacobian. Two examples of the matrix Λ are

Roe type diffusion operator:

$$\Lambda = \operatorname{diag}\left(|\lambda^1|, \ldots, |\lambda^m|\right), \tag{3.5}$$

where $\lambda^1, \ldots, \lambda^m$ are the eigenvalues of $\partial_{\mathbf{u}}\mathbf{f}(\mathbf{u}_{i+1/2})$;

Rusanov type diffusion operator:

$$\Lambda = \max\left(|\lambda^1|, \ldots, |\lambda^m|\right)\mathbf{I}, \tag{3.6}$$

with $\mathbf{I}$ being the identity matrix in $\mathbb{R}^{m\times m}$.

As the term $[\![\mathbf{v}]\!]_{i+1/2}$ is of the order of Δx, the scheme with flux (3.2) is in general only first-order accurate. This remains true even if we replace the entropy conservative flux $\widetilde{\mathbf{F}}$ in (3.2) with the very high-order entropy conservative flux (2.20).

3.2. **High-order diffusion operators.** In order to obtain a higher order accurate scheme, we need to perform a suitable reconstruction of the entropy variables $\mathbf{v}$. A k-th order ($k \in \mathbb{N}$) reconstruction produces a piecewise $(k-1)$-th degree polynomial function $\mathbf{v}_i(x)$. Denoting

$$\mathbf{v}_i^- = \mathbf{v}_i(x_{i-1/2}), \qquad \mathbf{v}_i^+ = \mathbf{v}_i(x_{i+1/2}), \qquad \langle\!\langle \mathbf{v} \rangle\!\rangle_{i+1/2} = \mathbf{v}_{i+1}^- - \mathbf{v}_i^+, \tag{3.7}$$

we define our higher-order (depending on the order of the reconstruction) numerical flux as

$$\mathbf{F}^k_{i+1/2} = \widetilde{\mathbf{F}}^{2p}_{i+1/2} - \frac{1}{2}\mathbf{D}_{i+1/2}\langle\!\langle \mathbf{v} \rangle\!\rangle_{i+1/2} \tag{3.8}$$

(compare to (3.2)). The number $p \in \mathbb{N}$ is chosen as $p = k/2$ if k is even and $p = (k+1)/2$ if k is odd. The flux $\widetilde{\mathbf{F}}^{2p}$ is the high order entropy conservative flux given by (2.20). The scheme with numerical flux (3.8) is k-th order accurate – its truncation error is $\mathcal{O}(\Delta x^k)$ for smooth solutions. However, the scheme with numerical flux (3.8) might not be entropy stable. We need to modify the reconstruction procedure to ensure entropy stability.

Lemma 3.2. *For each $i \in \mathbb{Z}$, let $R_{i+1/2} \in \mathbb{R}^{m\times m}$ be nonsingular, let $\Lambda_{i+1/2}$ be any nonnegative diagonal matrix and define the numerical diffusion matrix*

$$\mathbf{D}_{i+1/2} = R_{i+1/2}\Lambda_{i+1/2}R^\top_{i+1/2}. \tag{3.9}$$

Let $\mathbf{v}_i(x)$ be a polynomial reconstruction of the entropy variables in the cell I_i such that for each i, there exists a diagonal matrix $B_{i+1/2} \geq 0$ such that

$$\langle\!\langle \mathbf{v} \rangle\!\rangle_{i+1/2} = \left(R^\top_{i+1/2}\right)^{-1} B_{i+1/2}R^\top_{i+1/2}[\![\mathbf{v}]\!]_{i+1/2} \tag{3.10}$$

Then the scheme with numerical flux (3.8) *is entropy stable – its computed solutions satisfy the entropy dissipation estimate*

$$\frac{d}{dt}E(\mathbf{u}_i) + \frac{1}{\Delta x}\left(\widehat{Q}^k_{i+1/2} - \widehat{Q}^k_{i-1/2}\right) \leq 0, \tag{3.11}$$

where the numerical entropy flux function $\widehat{Q}^k$ is defined as

$$\widehat{Q}^k_{i+1/2} = \widetilde{Q}^{2p}_{i+1/2} - \frac{1}{2}\overline{\mathbf{v}}^\top_{i+1/2}\mathbf{D}_{i+1/2}\langle\!\langle \mathbf{v} \rangle\!\rangle_{i+1/2}$$

and $\widetilde{Q}^{2p}$ is defined in (2.21).

Proof. Multiplying the finite difference scheme (1.6) by $\mathbf{v}_i^\top$ and imitating the proof of Theorem 2.2 (see [28]), we obtain

$$\begin{aligned}\frac{d}{dt}E(\mathbf{u}_i) &= -\frac{1}{\Delta x}\left(\widetilde{Q}^{2p}_{i+1/2} - \widetilde{Q}^{2p}_{i-1/2}\right) + \frac{1}{2\Delta x}\left(\mathbf{v}_i^\top \mathbf{D}_{i+1/2}\langle\!\langle \mathbf{v}\rangle\!\rangle_{i+1/2} - \mathbf{v}_i^\top \mathbf{D}_{i-1/2}\langle\!\langle \mathbf{v}\rangle\!\rangle_{i-1/2}\right)\\ &= -\frac{1}{\Delta x}\left(\widehat{Q}^{k}_{i+1/2} - \widehat{Q}^{k}_{i-1/2}\right) - \frac{1}{4\Delta x}\left([\![\mathbf{v}]\!]^\top_{i+1/2}\mathbf{D}_{i+1/2}\langle\!\langle \mathbf{v}\rangle\!\rangle_{i+1/2} + [\![\mathbf{v}]\!]^\top_{i-1/2}\mathbf{D}_{i-1/2}\langle\!\langle \mathbf{v}\rangle\!\rangle_{i-1/2}\right).\end{aligned}$$

Suppressing vector and matrix indices $i+1/2$ for the moment, we have by (3.9) and (3.10)

$$[\![\mathbf{v}]\!]^\top \mathbf{D}\langle\!\langle \mathbf{v}\rangle\!\rangle = [\![\mathbf{v}]\!]^\top R\Lambda R^{-1}RBR^\top[\![\mathbf{v}]\!] = [\![\mathbf{v}]\!]^\top R\Lambda BR^\top[\![\mathbf{v}]\!] = \left(R^\top[\![\mathbf{v}]\!]\right)^\top \Lambda B\left(R^\top[\![\mathbf{v}]\!]\right) \geq 0$$

(since $B_{i+1/2} \geq 0$), and so

$$\frac{d}{dt}E(\mathbf{u}_i) \leq -\frac{1}{\Delta x}\left(\widehat{Q}^{k}_{i+1/2} - \widehat{Q}^{k}_{i-1/2}\right).$$

□

Remark 3.3. If the reconstructed variables satisfies (3.10), then the numerical flux (3.8) admits the equivalent representation

$$\mathbf{F}^k_{i+1/2} = \widetilde{\mathbf{F}}^{2p}_{i+1/2} - \frac{1}{2}R_{i+1/2}\Lambda_{i+1/2}B_{i+1/2}R^\top_{i+1/2}[\![\mathbf{v}]\!]_{i+1/2}.$$

This reveals the role of $B_{i+1/2}$ as limiting the amount of numerical diffusion: in smooth parts of the flow, we have $B_{i+1/2} \approx 0$, and we are left with the entropy conservative flux.

Although any R, Λ in (3.8) gives an entropy stable scheme, we choose Λ to be either the Rusanov (3.6) or Roe (3.5) matrices. Similarly, R is chosen as the matrix of eigenvectors of the flux Jacobian. The rationale for doing so is as follows. The Roe diffusion operator has the form $R|\Lambda|R^{-1}[\![\mathbf{u}]\!]$, where R and Λ are evaluated at the Roe average. In many cases there is some (possible different) intermediate state $\mathbf{u}_{i+1/2}$ such that $[\![\mathbf{u}]\!]_{i+1/2} = \mathbf{v}_\mathbf{u}[\![\mathbf{v}]\!]_{i+1/2}$, where $\mathbf{v}_\mathbf{u} = \partial_\mathbf{u}\mathbf{v}(\mathbf{u}_{i+1/2})$. Moreover, by a theorem due to Barth [1, Theorem 4], there exists a scaling of the column vectors of $R = R(\mathbf{u}_{i+1/2})$ such that $\mathbf{v}_\mathbf{u} = RR^\top$. Then

$$R|\Lambda|R^{-1}[\![\mathbf{u}]\!] \approx R|\Lambda|R^{-1}\mathbf{v}_\mathbf{u}[\![\mathbf{v}]\!] = R|\Lambda|R^\top[\![\mathbf{v}]\!].$$

This is precisely the form of our diffusion operator.

3.3. **Reconstruction procedure.** Lemma 3.2 provides sufficient conditions on the reconstruction for the scheme to be entropy stable. In this section, we will describe reconstruction procedures that satisfy the crucial condition (3.10). Assume for the moment that $\mathbf{v}_i, \mathbf{v}_{i+1}, \mathbf{v}_i^+, \mathbf{v}_{i+1}^-$ are given. Define the *scaled entropy variables*

$$\mathbf{w}_i^\pm = R^\top_{i\pm1/2}\mathbf{v}_i, \qquad \widetilde{\mathbf{w}}_i^\pm = R^\top_{i\pm1/2}\mathbf{v}_i^\pm.$$

The condition (3.10) now reads

$$\langle\!\langle \widetilde{\mathbf{w}}\rangle\!\rangle_{i+1/2} = B_{i+1/2}\langle\!\langle \mathbf{w}\rangle\!\rangle_{i+1/2}.$$

This is a component-wise condition; denoting the l-th component of $\mathbf{w}_i$ and $\widetilde{\mathbf{w}}_i$ by w_i^l and $\widetilde{w}_i^l$, respectively, the above condition is equivalent to

$$\begin{aligned}&\text{if} \quad \langle\!\langle w^l\rangle\!\rangle_{i+1/2} > 0 \quad &&\text{then} \quad \langle\!\langle \widetilde{w}^l\rangle\!\rangle_{i+1/2} \geq 0\\ &\text{if} \quad \langle\!\langle w^l\rangle\!\rangle_{i+1/2} < 0 \quad &&\text{then} \quad \langle\!\langle \widetilde{w}^l\rangle\!\rangle_{i+1/2} \leq 0\\ &\text{if} \quad \langle\!\langle w^l\rangle\!\rangle_{i+1/2} = 0 \quad &&\text{then} \quad \langle\!\langle \widetilde{w}^l\rangle\!\rangle_{i+1/2} = 0.\end{aligned} \tag{3.12}$$

We abbreviate this by writing

$$\operatorname{sign}\langle\!\langle \widetilde{w}^l\rangle\!\rangle_{i+1/2} = \operatorname{sign}\langle\!\langle w^l\rangle\!\rangle_{i+1/2}. \tag{3.13}$$

We term this highly non-linear structural property of the reconstruction the *sign property*. Reconstruction procedures that satisfy the sign property are presented following sections.

3.4. **2nd order TVD reconstruction.** We begin with the second-order case, which involves reconstruction with piecewise linear functions. For a fixed l, we denote the l-th component of the scaled entropy variable as w and define the undivided differences

$$\delta_{i+1/2} = \langle\!\langle w \rangle\!\rangle_{i+1/2}. \tag{3.14}$$

Let ϕ be some slope limiter with the symmetry property $\phi(\theta^{-1}) = \phi(\theta)\theta^{-1}$ (see [19]). Define the quotients

$$\theta_i^- = \frac{\delta_{i+1/2}}{\delta_{i-1/2}} \qquad \text{and} \qquad \theta_i^+ = \frac{\delta_{i-1/2}}{\delta_{i+1/2}}.$$

We denote the "slope" in grid cell I_i by

$$\sigma_i = \frac{1}{\Delta x}\phi(\theta_i^-)\delta_{i-1/2} = \frac{1}{\Delta x}\phi(\theta_i^+)\delta_{i+1/2}.$$

(The second equality follows from the symmetry of ϕ.) Hence, the reconstructed values at the left and right cell interfaces of grid cell I_i are given by $\widetilde{w}_i^- = w_i^- - \frac{1}{2}\phi(\theta_i^-)\delta_{i-1/2}$ and, respectively, $\widetilde{w}_i^+ = w_i^+ + \frac{1}{2}\phi(\theta_i^+)\delta_{i+1/2}$. We obtain

$$\langle\!\langle \widetilde{w} \rangle\!\rangle_{i+1/2} = w_{i+1}^- - w_i^+ - \frac{1}{2}\left(\phi(\theta_i^+) + \phi(\theta_{i+1}^-)\right)\delta_{i+1/2} = \left(1 - \frac{1}{2}\left(\phi(\theta_i^+) + \phi(\theta_{i+1}^-)\right)\right)\delta_{i+1/2}.$$

Recalling the definition of δ (3.14), we find that the sign property (3.12) is satisfied *if and only if* $\phi(\theta) \le 1$ for all $\theta \in \mathbb{R}$. It is easily seen that the *minmod* limiter, given by

$$\phi^{\mathrm{mm}}(\theta) = \begin{cases} 0 & \text{if } \theta < 0 \\ \theta & \text{if } 0 \le \theta \le 1 \\ 1 & \text{otherwise} \end{cases} \tag{3.15}$$

satisfies $\phi(\theta) \le 1$. In fact, the minmod limiter is the *only* symmetric TVD limiter that satisfies the sign property. However, non-TVD limiters might satisfy this condition. One example is the second-order version of the ENO reconstruction procedure [12], which can be expressed in terms of the flux limiter

$$\phi(\theta) = \begin{cases} \theta & \text{if } -1 \le \theta \le 1 \\ 1 & \text{else,} \end{cases} \tag{3.16}$$

This limiter is both symmetric and satisfies $\phi(\theta) \le 1$, thus ensuring the sign property. Indeed, the ENO limiter may be viewed as a symmetric extension of the minmod limiter (3.15) into the negative θ-axis.

3.5. **ENO reconstruction procedure.** The above discussion reveals that the second-order version of the ENO reconstruction procedure satisfies the sign property, encouraging us to investigate whether the sign property holds for higher-order versions of the ENO procedure.

As described in [12], the ENO procedure for k-th order accurate reconstructions point values w_i amounts to selecting a stencil of k points $\{x_{i-r_i}, \dots, x_{i-1-r_i+k}\}$. The integer $r_i \in \{0, \dots, k-1\}$ is the left shift index of the stencil. We may determine the left-displacement index r_i for the grid cell I_i by using values of the undivided differences $\{\delta_{j+1/2}\}_{j=i-k+1}^{i+k-1}$ of w_i.

The question of whether the ENO procedure satisfies the sign property was answered in the recent paper [9].

Theorem 3.4 (Fjordholm, Mishra, Tadmor [9])**.** *Let $k \in \mathbb{N}$ and let $\omega_i^+, \omega_{i+1}^-$ be the left and right values at the cell interface $x_{i+1/2}$, obtained through a k-th order ENO reconstruction of the point values ω_i of a function ω. Then the reconstruction satisfies the sign property:*

$$\operatorname{sign}\big(\omega_{i+1}^- - \omega_i^+\big) = \operatorname{sign}\big(\omega_{i+1} - \omega_i\big). \tag{3.17}$$

Furthermore, we have

$$\frac{\omega_{i+1}^- - \omega_i^+}{\omega_{i+1} - \omega_i} \le \mathcal{C}_k \tag{3.18}$$

for a constant $\mathcal{C}_k$ that only depends on k.

As the values we are reconstructing, the scaled entropy variables, are centered at cell interfaces, we must modify the reconstruction method somewhat. Given the interface values of each component w of the scaled entropy variables $\mathbf{w}$ for a fixed grid cell I_i, define the point value $\mu_i^i = w_i^-$, and inductively

$$\begin{aligned} \mu_{j+1}^i &= \mu_j^i + \delta_{j+1/2} \qquad (j = i, i+1, \dots) \\ \mu_{j-1}^i &= \mu_j^i - \delta_{j-1/2} \qquad (j = i, i-1, \dots). \end{aligned}$$

Similarly, we define $\nu_i^i = w_i^+$ and

$$\begin{aligned} \nu_{j+1}^i &= \nu_j^i + \delta_{j+1/2} \qquad (j = i, i+1, \dots) \\ \nu_{j-1}^i &= \nu_j^i - \delta_{j-1/2} \qquad (j = i, i-1, \dots). \end{aligned}$$

Then μ and ν retain the cell interface jumps of w,

$$[\![\mu^i]\!]_{j+1/2} = [\![\nu^i]\!]_{j+1/2} = \delta_{j+1/2} = \langle\!\langle w \rangle\!\rangle_{j+1/2} \qquad \text{for all } j. \tag{3.19}$$

As ν and μ have the same jump at a cell interface, we have

$$\mu_j^{i+1} = \nu_j^i \qquad \text{for all } j. \tag{3.20}$$

Since the divided differences of μ and ν coincide with those obtained with $\delta_{j+1/2}$ as described above, the ENO stencil selection procedure will yield exactly the same stencil (in other words, the same left-displacement index r_i) whether μ or ν is provided as input data for the procedure. Let $p^i(x)$ and $q^i(x)$, respectively, be the unique $(k-1)$-th order polynomial interpolations for the values μ^i and ν^i on the above stencil. Since

$$\mu_j^i = \nu_j^i + (\mu_i^i - \nu_i^i) \qquad \text{for all } j,$$

we have

$$p^i(x) = q^i(x) + (\mu_i^i - \nu_i^i) \qquad \text{for all } x.$$

Hence, the interpolation polynomial need only be computed once for both the left and the right interfaces. Finally, we obtain left and right reconstructed values:

$$\widetilde{w}_i^- = p^i(x_{i-1/2}) \qquad \text{and} \qquad \widetilde{w}_i^+ = q^i(x_{i+1/2}).$$

This process is repeated *in each grid cell* I_i and *for each component* of $\mathbf{w}_i^{\pm}$.

Corollary 3.5. *The reconstructed values* $\widetilde{w}_i^{\pm}$ *satisfy the sign property* (3.12).

Proof. Fix $i \in \mathbb{Z}$ and denote the (standard) ENO reconstructed polynomial of point values $\{\mu_j^{i+1}\}_{j\in\mathbb{Z}}$ in grid cell j by $h^j(x)$. Because of (3.20), the polynomial q^i is precisely equal to h^j. Obviously, $p^{i+1} = h^{i+1}$. Hence,

$$\langle\!\langle \widetilde{w} \rangle\!\rangle_{i+1/2} = p^{i+1}(x_{i+1/2}) - q^i(x_{i+1/2}) = h^{i+1}(x_{i+1/2}) - h^i(x_{i+1/2}),$$

which by Theorem 3.4 has the same sign as $\mu_{i+1}^{i+1} - \mu_i^{i+1}$, which by definition equals $\langle\!\langle w \rangle\!\rangle_{i+1/2}$. □

4. Arbitrarily high order accurate entropy stable schemes.

We combine the high-order accurate entropy conservative fluxes (2.20) with a numerical diffusion operator based on ENO reconstruction of the scaled entropy variables. This defines an arbitrarily high-order accurate entropy stable scheme.

Theorem 4.1. *For any* $k \geq 1$, *let* $2p = k$ *(if* k *is even) or* $2p = k+1$ *(if* k *is odd). Define the entropy conservative flux* $\widetilde{\mathbf{F}}^{2p}$ *by* (2.20). *Let* $\langle\!\langle \mathbf{v} \rangle\!\rangle$ *in* (3.8) *be defined by the* k*-th order accurate ENO reconstruction procedure (as outlined in Section 3.5). Then the finite difference scheme with numerical flux* (3.8) *is*

(i) $(k-1)$*-th order accurate for smooth solutions.*
(ii) entropy stable – computed solutions satisfy the discrete entropy inequality (3.11).

Proof. The proof of (i) is delayed to Appendix A. (ii) is a direct consequence of Lemma 3.2; condition (3.10) of that lemma follows from Corollary 3.5. □

Remark 4.2. Note that we are only able to prove that the scheme is $(k-1)$-th order accurate – there is a nonzero term of order Δx^{k-1} in the diffusion operator that does not vanish. However, in practice we see behavior of order Δx^k, and therefore chose not to alter our scheme.

Our scheme combines entropy conservative flux (2.20) with ENO based numerical diffusion operator in (3.8); hence, we term them as *TeCNO schemes*.

We have the following convergence result for TeCNO schemes approximating linear symmetrizable systems.

Theorem 4.3. *Consider a linear system, i.e,* $\mathbf{f}(\mathbf{u}) = \mathbf{A}\mathbf{u}$ *for a constant* $m \times m$ *matrix* $\mathbf{A}$*, and assume that there exists a symmetric positive definite matrix* $\mathbf{S}$ *such that* $\mathbf{SA}$ *is symmetric. Let* $\mathbf{u}_i(t)$ *be the solution computed with the scheme with flux* (3.8)*, based on the two-point entropy conservative flux* (2.9)*, and define* $\mathbf{u}^{\Delta x}(x,t) = \mathbf{u}_i(t)$ *for* $x \in I_i$*. Then* $\mathbf{u}^{\Delta x} \rightharpoonup \mathbf{u}$ *(up to a subsequence) in* $L^2([0,T], L^2(\mathbb{R}))$ *as* $\Delta x \to 0$*, where* $\mathbf{u}$ *is the unique weak solution of the linear system.*

The proof of this theorem is given in Appendix B. Note that this convergence result holds even when the solution of the linear system is discontinuous. It is straightforward to generalize this result to linear symmetrizable systems with variable (but smooth) coefficients.

At the time of writing, we are unable to obtain a similar convergence result for scalar non-linear conservation laws (except for first-order schemes) due to technical complications. However, using a specific entropy function, we obtain an L^∞ bound. Let $u = \mathbf{u}$ denote the computed solution, and let $a, b \in \mathbb{R}$ be such that $a < u_0(x) < b$ for all $x \in \mathbb{R}$. Then

$$E(u) = -\log(b-u) - \log(u-a) \tag{4.1}$$

is convex and hence serves as an entropy function. The corresponding entropy conservative flux is easily found with the formula (2.2).

Lemma 4.4. *Solutions computed with the TeCNO flux* (3.8) *for the entropy* (4.1) *satisfy the* L^∞ *estimate*

$$a < u_i(T) < b \qquad \forall\ i \in \mathbb{Z},\ T \geq 0. \tag{4.2}$$

Proof. Integrating the entropy inequality (3.11) over $i \in \mathbb{Z}$ and $t \in [0,T]$ gives $\Delta x \sum_i E(u_i(T)) \leq \Delta x \sum_i E(u_0(x_i))$. In particular, since $E(u) \geq -2\log\left(\frac{b-a}{2}\right)$ for all $u \in (a,b)$, we have $E(u_i(T)) \leq C$ for all $i \in \mathbb{Z}$. Since $E(u) \to \infty$ as $u \to a, b$, there must necessarily be some $C_2 > 0$ such that $u_i(T) \leq C_2$ for all $i \in \mathbb{Z}$. □

5. Numerical experiments

We test the following schemes:

ENOk: k-th order accurate standard ENO scheme in the MUSCL formulation [12].
TeCNOk: k-th order accurate entropy stable scheme with numerical flux (3.8)

for $k = 2, 3, 4$ and 5 on a suite of numerical experiments involving scalar equations as well as systems. The ENO-MUSCL and TeCNO schemes are semi-discrete and are integrated in time with a 2nd, 3rd or 4th order explicit Runge-Kutta method. In all experiments we use a CFL number of 0.45.

5.1. Linear advection equation.

We consider the linear advection equation

$$u_t + a u_x = 0, \tag{5.1}$$

with wavespeed $a = 1$ in the domain $[-1, 1]$ with periodic boundary conditions. The initial data is $u_0(x) = \sin(\pi x)$. The entropy function in this case is the total energy $E(u) = u^2/2$ and the entropy variable is $v = u$. The entropy conservative flux $\widetilde{F}$ is the average flux (2.9). We use the advection velocity a as the coefficient of diffusion by setting $D \equiv a$ in (3.8). The 4th and 5th order ENO and TeCNO schemes are compared in Figure 1. To illustrate the differences between the schemes, the solutions are computed on a very coarse mesh of 20 points and the simulation is performed for a large time $T = 10$. The results show that the fifth order schemes are more accurate than the fourth order schemes. Furthermore, the TeCNO scheme is clearly more accurate than the corresponding standard ENO scheme of the same order.

5.2. Burgers' equation.

Next we consider Burgers' equation

$$u_t + \left(\frac{u^2}{2}\right)_x = 0. \tag{5.2}$$

The computational domain is $[-1, 1]$ with periodic boundary conditions, and we use the initial data $u_0(x) = 1 + \frac{1}{2}\sin(\pi x)$. We choose to use the logarithmic entropy function $E(U) = -\log(b-u) - \log(u-a)$ with constants

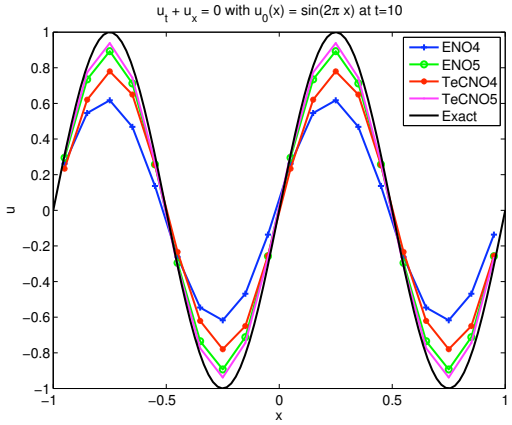

FIGURE 1. Solution at $t = 10$ computed with fourth- and fifth-order accurate ENO and TeCNO schemes for the linear advection equation.

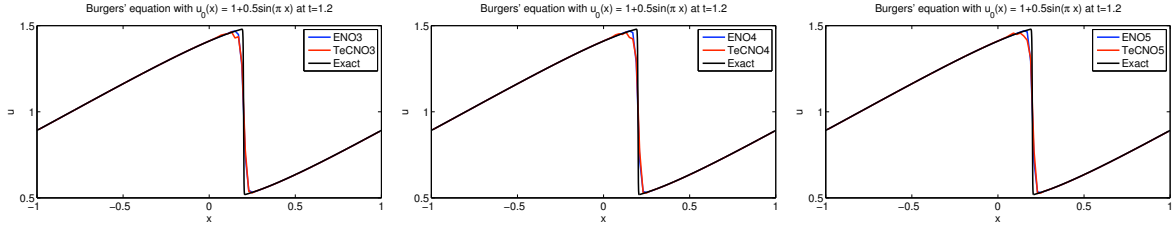

FIGURE 2. Approximate solutions computed with third, fourth and fifth order accurate ENO and TeCNO schemes for Burgers' equation at time $t = 1.2$ on a mesh of 100 points.

$a = 0$ and $b = 2$ in order to bound the initial data. The entropy conservative flux is given by

$$\widetilde{F}_{i+1/2} = \frac{u_i u_{i+1}}{2} + \frac{\dfrac{b}{(b-u)^{\ln}_{i+1/2}} - \dfrac{a}{(u-a)^{\ln}_{i+1/2}} - 2}{\dfrac{1}{(b-u_{i+1})(b-u_i)} + \dfrac{1}{(u_{i+1}-a)(u_i-a)}}. \tag{5.3}$$

Numerical results are shown in Figure 2. The initial sine wave breaks down into a shock and a rarefaction wave. In this example, the ENO and TeCNO schemes show comparable resolution at the discontinuities. There is no visible gain in using a higher order scheme at this mesh size.

5.3. **The wave equation.** We consider the one-dimensional wave equation

$$\begin{aligned} h_t + c m_x &= 0 \\ m_t + c h_x &= 0 \end{aligned} \tag{5.4}$$

and let $c = 1$. The wave equation is a linear symmetric system and has the energy $E(\mathbf{u}) = \frac{1}{2}\left(h^2 + m^2\right)$ as entropy function, with entropy variables $\mathbf{v} = \mathbf{u}$. The resulting entropy conservative flux is the average flux (2.9). We use the diffusion matrix

$$\mathbf{D} = \begin{bmatrix} c & 0 \\ 0 & c \end{bmatrix},$$

in the numerical diffusion operator in (3.8). The ENO-MUSCL scheme uses reconstruction along characteristics.

5.3.1. *Smooth waves.* Consider the wave equation (5.4) with initial data $h(x, 0) = \sin(4\pi x)$ and $m(x, 0) \equiv 0$ in the domain $x \in [-1, 1]$ with periodic boundary conditions. We compute L^1 errors for all the schemes (computed with respect to the exact solution) at time $t = 1$ and show the convergence plot in Figure 3. The figures show that both the ENO and TeCNO schemes converge at the claimed orders of accuracy. The TeCNO schemes have consistently lower error amplitudes than the ENO schemes at the same order.

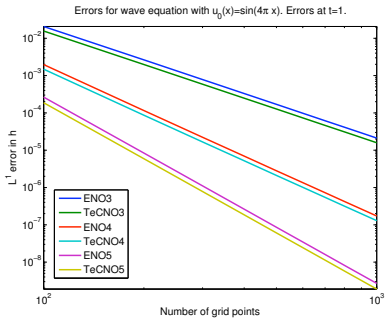

FIGURE 3. L^1 errors in h for the wave equation with third, fourth and fifth order ENO and TeCNO schemes for the wave equation with sine initial data.

5.3.2. *Contact discontinuities.* We consider the wave equation (5.4) with initial data

$$h(x,0) = \begin{cases} x-1 & \text{if } x < 0 \\ 1-x & \text{if } x > 0 \end{cases} \qquad m(x,0) = 0$$

on the domain $x \in [-1,1]$ with periodic boundary conditions. The solution features an initial jump discontinuity at $x = 0$ which breaks into two linear (contact) discontinuities. Computed solutions at time $t = 1.5$ for each scheme, on a mesh of 100 points, is displayed in Figure 4. The two methods resolve the flow with a comparable level of accuracy.

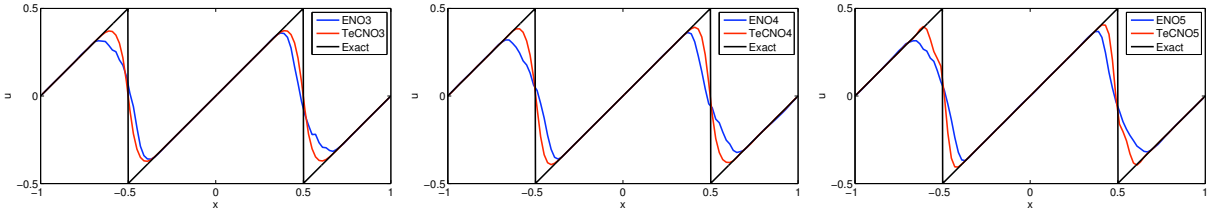

FIGURE 4. The height for the wave equation with discontinuous initial data, computed with the third, fourth and fifth order ENO and TeCNO schemes at time $t = 1.5$ on a mesh of 100 points.

5.4. **The shallow water equations.** We consider the shallow water equations (2.10) with entropy function, entropy flux and entropy variables given in (2.11), (2.12). For the TeCNO schemes we use the two-point entropy conservative flux (2.13). The numerical diffusion operator in (3.8) is of the Roe type (3.5) with eigenvalues and eigenvectors of the Jacobian evaluated at the arithmetic average of the left and right states. The ENO schemes use a MUSCL approach with the Rusanov numerical flux. The gravitational constant is set to $g = 1$.

5.4.1. *A dambreak problem.* We consider a dambreak problem for the shallow water equations with initial data

$$h(x,0) = \begin{cases} 1.5 & \text{if } |x| < 0.2 \\ 1 & \text{if } |x| > 0.2 \end{cases} \qquad hu(x,0) = 0$$

for $x \in [-1,1]$ with periodic boundary conditions The exact solution consists of two shocks separated by two rarefactions. We display computed heights in Figure 5. The figure reveals that the TeCNO schemes are comparable to the ENO schemes of corresponding order: the TeCNO schemes approximate the shocks more sharply than the ENO schemes, whereas the ENO schemes resolve the rarefactions more accurately, albeit with small oscillations. The TeCNO schemes resolve the rarefactions without any noticeable oscillations.

5.5. **Euler equations.** We consider the Euler equations, as described in Section 2.1.4. We define the TeCNO scheme with entropy conservative flux given by (2.19) and diffusion matrix being of the Roe type (3.5). The eigenvalues and eigenvectors of the Jacobian are computed at the arithmetic average of the left and right states. The ENO-MUSCL schemes use the standard Roe numerical flux.

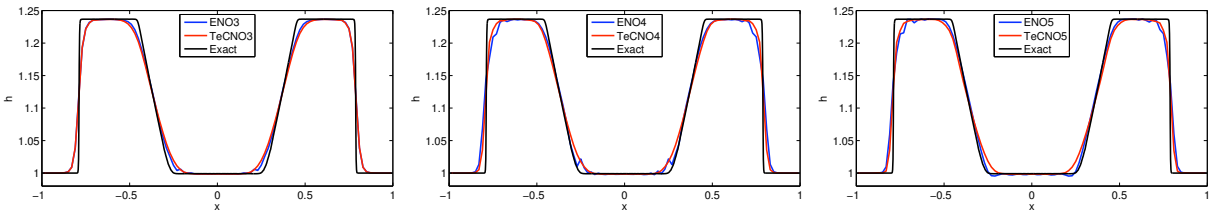

FIGURE 5. Computed heights for the shallow water dam break problem with third, fourth and fifth order ENO and TeCNO schemes at $t = 0.4$ on a mesh of 100 points.

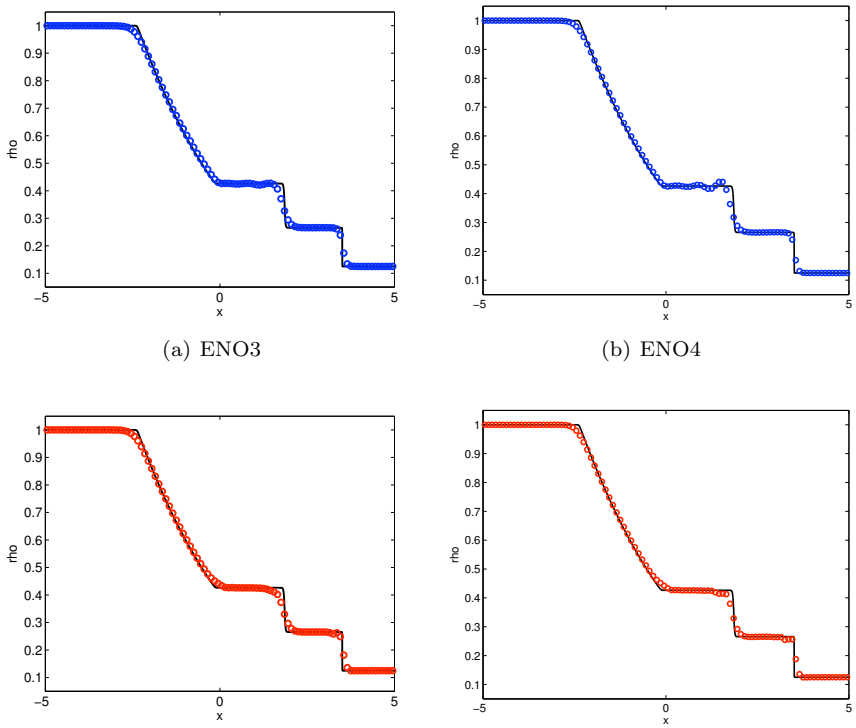

(a) ENO3 (b) ENO4

(c) TeCNO3 (d) TeCNO4

FIGURE 6. Comparing ENO (blue circles) and TeCNO (red circles) with the reference solution (black line) for the Sod shock tube. Density at $t = 1.3$ on a mesh of 100 points is plotted.

5.5.1. *Sod shock tube.* The Sod shock tube experiment is the Riemann problem

$$\mathbf{u}(x,0) = \begin{cases} \mathbf{u}_L & \text{if } x < 0 \\ \mathbf{u}_R & \text{otherwise,} \end{cases} \tag{5.5}$$

with

$$\begin{bmatrix} \rho_L \\ u_L \\ p_L \end{bmatrix} = \begin{bmatrix} 1 \\ 0 \\ 1 \end{bmatrix}, \qquad \begin{bmatrix} \rho_R \\ u_R \\ p_R \end{bmatrix} = \begin{bmatrix} 0.125 \\ 0 \\ 0.1 \end{bmatrix}$$

in the computational domain $x \in [-5, 5]$. The initial discontinuity breaks into a left-going rarefaction wave, a right-going shock wave and a right-going contact discontinuity. The computed density with the ENO3, ENO4, TeCNO3 and TeCNO4 schemes at time $t = 1.3$ on a mesh of 100 points is shown in Figure 6. The results show that the ENO and TeCNO schemes are quite good at resolving the waves. The ENO4 scheme is slightly oscillatory behind the contact whereas the TeCNO3 and TeCNO4 schemes resolve all the waves without any noticeable oscillations.

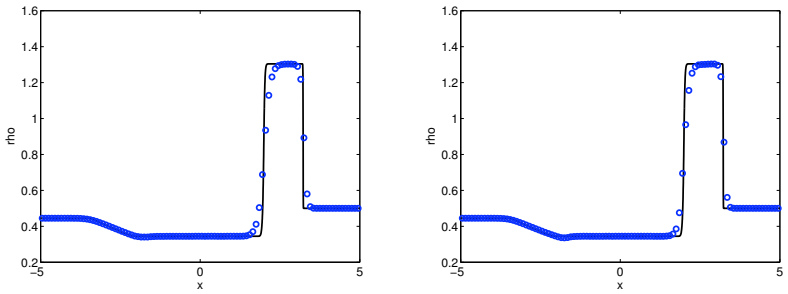

(a) ENO3 (b) ENO4

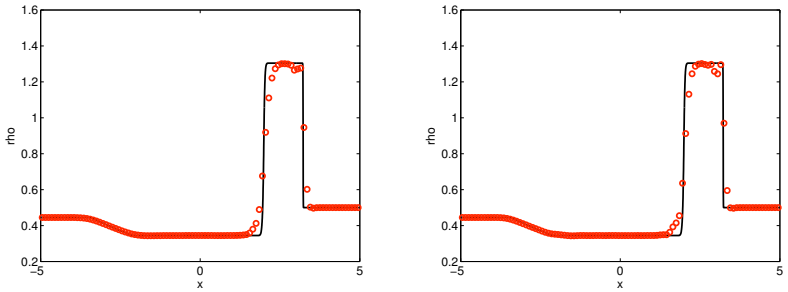

(c) TeCNO3 (d) TeCNO4

FIGURE 7. Comparing ENO (blue circles) and TeCNO (red circles) with exact solution (black line) for the Lax shock tube. The density at time $t = 1.3$ on a mesh of 100 points is plotted.

5.5.2. *Lax shock tube.* We consider the Euler equations in the computational domain $[-5, 5]$ with Riemann initial data (5.5) given by

$$\begin{bmatrix} \rho_L \\ u_L \\ p_L \end{bmatrix} = \begin{bmatrix} 0.445 \\ 0.698 \\ 3.528 \end{bmatrix}, \qquad \begin{bmatrix} \rho_R \\ u_R \\ p_R \end{bmatrix} = \begin{bmatrix} 0.5 \\ 0 \\ 0.571 \end{bmatrix}.$$

The computed density at $t = 1.3$ on a mesh of 100 points is shown in Figure 7. The results for ENO and TeCNO schemes are very similar in this experiment. There are slight oscillations behind the shock for the TeCNO schemes.

5.5.3. *Shock-Entropy wave interaction.* This numerical example was proposed by Shu and Osher in [24] and is a good test of a scheme's ability to resolve a complex solution with both strong and weak shocks and highly oscillatory but smooth waves. The computational domain is $[-5, 5]$ and we use with initial data

$$\mathbf{u}(x, 0) = \begin{cases} \mathbf{u}_L & \text{if } x < -4 \\ \mathbf{u}_R & \text{otherwise,} \end{cases}$$

with

$$\begin{bmatrix} \rho_L \\ u_L \\ p_L \end{bmatrix} = \begin{bmatrix} 3.857143 \\ 2.629369 \\ 10.33333 \end{bmatrix}, \qquad \begin{bmatrix} \rho_R \\ u_R \\ p_R \end{bmatrix} = \begin{bmatrix} 1 + \varepsilon \sin(5x) \\ 0 \\ 1 \end{bmatrix}.$$

As a reference solution, we compute with the ENO3 scheme on a mesh of 1600 grid points. The approximate solutions are computed on a mesh of 200 grid points, corresponding to about 7 grid points for each period of the entropy waves. The solution computed by the ENO and TeCNO schemes are displayed in Figure 8. There are very minor differences between the ENO and TeCNO schemes of the same order. The test also illustrates that the higher order schemes perform better than the low order schemes.

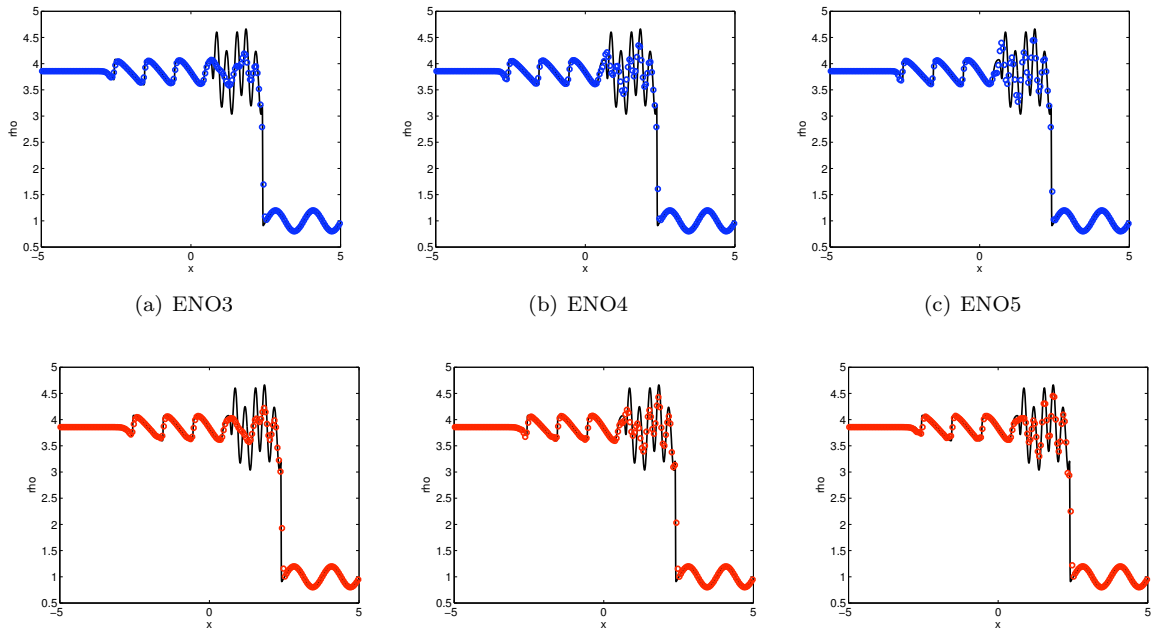

(a) ENO3 (b) ENO4 (c) ENO5

(d) TeCNO3 (e) TeCNO4 (f) TeCNO5

FIGURE 8. Comparing ENO (blue circles) and TeCNO (red circles) with a reference solution (black line) on the Shu-Osher shock-entropy wave interaction problem. The plotted quantity is the density at time $t = 1.8$ on a mesh of 200 points.

5.6. **Conclusions.** The numerical experiments show that the TeCNO schemes achieve the claimed orders of accuracy for smooth solutions and resolve shocks and other waves robustly. They are comparable to the standard ENO schemes of the same order.

6. Multi-dimensional problems

The arbitrary-order entropy stable TeCNO schemes can easily be extended to rectangular meshes in several space dimensions. We present a brief description of such schemes and omit details as they are very similar to the one-dimensional case.

6.1. **Continuous setting.** For simplicity, we concentrate on systems of conservation laws in two space dimensions:

$$\begin{aligned} \mathbf{u}_t + \mathbf{f}(\mathbf{u})_x + \mathbf{g}(\mathbf{u})_y = 0 \qquad & \forall\ (x,y,t) \in \mathbb{R}\times\mathbb{R}\times\mathbb{R}_+, \\ \mathbf{u}(x,y,0) = \mathbf{u}_0(x,y) \qquad & \forall\ (x,y) \in \mathbb{R}\times\mathbb{R}. \end{aligned} \tag{6.1}$$

Here, $\mathbf{u} : \mathbb{R}\times\mathbb{R}\times\mathbb{R}_+ \to \mathbb{R}^m$ is the vector of unknowns and $\mathbf{f}, \mathbf{g}$ are flux vectors in the x- and y-directions, respectively. We assume that there exists a convex function $E : \mathbb{R}^m \to \mathbb{R}$ and functions $Q^x, Q^y : \mathbb{R}^m \to \mathbb{R}$ such that

$$\partial_{\mathbf{u}} Q^x(\mathbf{u}) = \mathbf{v}^\top \partial_{\mathbf{u}} \mathbf{f}(\mathbf{u}), \qquad \partial_{\mathbf{u}} Q^y(\mathbf{u}) = \mathbf{v}^\top \partial_{\mathbf{u}} \mathbf{g}(\mathbf{u}). \tag{6.2}$$

Again, the entropy variables are defined as $\mathbf{v} = \partial_{\mathbf{u}} E(\mathbf{u})$. Entropy solutions of (6.1) satisfy the entropy inequality

$$E(\mathbf{u})_t + Q^x(\mathbf{u})_x + Q^y(\mathbf{u})_y \le 0 \tag{6.3}$$

(in the sense of distributions). We will design arbitrary-order accurate finite difference schemes that satisfy a discrete version of (6.3).

6.2. **Entropy stable finite difference schemes.** We consider a (uniform) Cartesian mesh in $\mathbb{R}^2$ consisting of mesh points $(x_i, y_j) = (i\Delta x, j\Delta y)$ for $i, j \in \mathbb{Z}$ and $\Delta x, \Delta y > 0$. Denoting the midpoints as

$$x_{i+1/2,j} = \frac{x_i + x_{i+1}}{2}, \quad y_{i,j+1/2} = \frac{y_j + y_{j+1}}{2},$$

a semi-discrete conservative finite difference scheme for (6.1) solves for point values $\mathbf{u}_{i,j} \approx \mathbf{u}(x_i, y_j)$, and can be written as

$$\frac{d}{dt}\mathbf{u}_{i,j}(t) + \frac{1}{\Delta x}\left(\mathbf{F}_{i+1/2,j}(t) - \mathbf{F}_{i-1/2,j}(t)\right) + \frac{1}{\Delta y}\left(\mathbf{G}_{i,j+1/2}(t) - \mathbf{G}_{i,j-1/2}(t)\right) = 0. \tag{6.4}$$

Here, $\mathbf{F}, \mathbf{G}$ are numerical flux functions that are consistent with $\mathbf{f}$ and $\mathbf{g}$, respectively. We suppress the t dependence of all quantities below for notational convenience. We will use the notation

$$\begin{aligned} [\![a]\!]_{i+1/2,j} &= a_{i+1,j} - a_{i,j}, & [\![a]\!]_{i,j+1/2} &= a_{i,j+1} - a_{i,j}, \\ \overline{a}_{i+1/2,j} &= \frac{a_{i,j} + a_{i+1,j}}{2}, & \overline{a}_{i,j+1/2} &= \frac{a_{i,j} + a_{i,j+1}}{2}. \end{aligned}$$

For any integer $k \geq 1$, the k-th order accurate TeCNO numerical fluxes are defined as

$$\mathbf{F}_{i+1/2,j} = \widetilde{\mathbf{F}}^{2p}_{i+1/2,j} - \frac{1}{2}\mathbf{D}^x_{i+1/2,j}\langle\!\langle \mathbf{v} \rangle\!\rangle_{i+1/2,j}, \qquad \mathbf{G}_{i,j+1/2} = \widetilde{\mathbf{G}}^{2p}_{i,j+1/2} - \frac{1}{2}\mathbf{D}^y_{i,j+1/2}\langle\!\langle \mathbf{v} \rangle\!\rangle_{i,j+1/2}. \tag{6.5}$$

The fluxes $\widetilde{\mathbf{F}}^{2p}, \widetilde{\mathbf{G}}^{2p}$, matrices $\mathbf{D}^x, \mathbf{D}^y$ and vectors $\langle\!\langle \mathbf{v} \rangle\!\rangle_{i+1/2,j}, \langle\!\langle \mathbf{v} \rangle\!\rangle_{i,j+1/2}$ are described below.

6.2.1. *High-order entropy conservative fluxes.* The setting of entropy conservative schemes is completely analogous to the one-dimensional case [28]. Two-point entropy conservative fluxes $\widetilde{\mathbf{F}}, \widetilde{\mathbf{G}}$ are chosen so that they satisfy

$$[\![\mathbf{v}]\!]^\top_{i+1/2,j}\widetilde{\mathbf{F}}_{i+1/2,j} = [\![\psi^x]\!]_{i+1/2,j}, \qquad [\![\mathbf{v}]\!]^\top_{i,j+1/2}\widetilde{\mathbf{G}}_{i,j+1/2} = [\![\psi^y]\!]_{i,j+1/2} \tag{6.6}$$

for all i, j, where the entropy potentials are defined as

$$\psi^x = \mathbf{v}^\top \mathbf{f} - Q^x, \qquad \psi^y = \mathbf{v}^\top \mathbf{g} - Q^y. \tag{6.7}$$

Analogously to the one-dimensional case, solutions computed with the entropy conservative fluxes (6.6) satisfy the entropy equality

$$\frac{d}{dt}E(\mathbf{u}_{i,j}) + \frac{1}{\Delta x}\left(\widetilde{Q}^x_{i+1/2,j} - \widetilde{Q}^x_{i-1/2,j}\right) + \frac{1}{\Delta y}\left(\widetilde{Q}^y_{i,j+1/2} - \widetilde{Q}^y_{i-1/2,j}\right) = 0,$$

where

$$\begin{aligned} \widetilde{Q}^x_{i+1/2,j} &= \widetilde{Q}^x(\mathbf{u}_{i,j}, \mathbf{u}_{i+1,j}) = \frac{1}{2}\left(\mathbf{u}_{i,j} + \mathbf{u}_{i+1,j}\right)^\top \widetilde{\mathbf{F}}(\mathbf{u}_{i,j}, \mathbf{u}_{i+1,j}) - \frac{1}{2}(\psi^x_{i,j} + \psi^x_{i+1,j}), \\ \widetilde{Q}^y_{i,j+1/2} &= \widetilde{Q}^y(\mathbf{u}_{i,j}, \mathbf{u}_{i,j+1}) = \frac{1}{2}\left(\mathbf{u}_{i,j} + \mathbf{u}_{i,j+1}\right)^\top \widetilde{\mathbf{G}}(\mathbf{u}_{i,j}, \mathbf{u}_{i,j+1}) - \frac{1}{2}(\psi^y_{i,j} + \psi^y_{i,j+1}). \end{aligned}$$

The relations (6.6) are identical to the relation (2.2) in one space dimension. Hence, two-point entropy conservative fluxes like (2.5) and (2.6) can be easily adapted to this setting. We can obtain explicit and algebraically simple solutions of (6.6) in a manner similar to Section 2.

Given an integer $k \geq 1$, let $2p = k$ if k is even and $2p = k+1$ if k is odd. The high-order entropy conservative fluxes $\widetilde{\mathbf{F}}^{2p}, \widetilde{\mathbf{G}}^{2p}$ are

$$\widetilde{\mathbf{F}}^{2p}_{i+1/2,j} = \sum_{r=1}^{p}\alpha^p_r \sum_{s=0}^{r-1}\widetilde{\mathbf{F}}(\mathbf{u}_{i-s,j}, \mathbf{u}_{i-s+r,j}), \qquad \widetilde{\mathbf{G}}^{2p}_{i,j+1/2} = \sum_{r=1}^{p}\alpha^p_r \sum_{s=0}^{r-1}\widetilde{\mathbf{G}}(\mathbf{u}_{i,j-s}, \mathbf{u}_{i,j-s+r}), \tag{6.8}$$

where the constants α^p_r are the same as in (2.20). Solutions computed with these fluxes satisfy an entropy equality with numerical entropy fluxes

$$\widetilde{Q}^{x,2p}_{i+1/2,j} = \sum_{r=1}^{p}\alpha^p_r \sum_{s=0}^{r-1}\widetilde{Q}^x(\mathbf{u}_{i-s,j}, \mathbf{u}_{i-s+r,j}), \qquad \widetilde{Q}^{y,2p}_{i+1/2,j} = \sum_{r=1}^{p}\alpha^p_r \sum_{s=0}^{r-1}\widetilde{Q}^y(\mathbf{u}_{i,j-s}, \mathbf{u}_{i,j-s+r}).$$

6.2.2. *ENO-based numerical diffusion operators.* The multidimensional reconstruction procedure is performed precisely as in the one-dimensional case, dimension by dimension. For each pair (i,j), let $R^x_{i+1/2,j}$, $R^y_{i,j+1/2}$ be the eigenvector matrices of $\partial_{\mathbf{u}}\mathbf{f}(\mathbf{u}_{i+1/2,j})$, $\partial_{\mathbf{u}}\mathbf{g}(\mathbf{u}_{i,j+1/2})$, where $\mathbf{u}_{i+1/2,j}$ and $\mathbf{u}_{i,j+1/2}$ are any intermediate states. For each fixed j, we reconstruct entropy variables $\{\mathbf{v}_{i,j}\}_{i\in\mathbb{Z}}$ along $R^x_{i+1/2,j}$ as in Section 3.5, obtaining jumps in reconstructed values $\langle\!\langle \mathbf{v}\rangle\!\rangle_{i+1/2,j}$. Next, i is kept fixed, and $\{\mathbf{v}_{i,j}\}_{j\in\mathbb{Z}}$ is reconstructed along $R^y_{i,j+1/2}$ to obtain jumps $\langle\!\langle \mathbf{v}\rangle\!\rangle_{i,j+1/2}$. This completes the description of the TeCNO numerical fluxes (6.5).

Theorem 6.1. *The TeCNO scheme* (6.4), (6.5) *is*

(i) k-th order accurate for smooth solutions.
(ii) entropy stable – computed solutions satisfy

$$\frac{d}{dt}E(\mathbf{u}_{i,j}) + \frac{1}{\Delta x}\left(\widehat{Q}^{x,2p}_{i+1/2,j} - \widehat{Q}^{x,2p}_{i-1/2,j}\right) + \frac{1}{\Delta y}\left(\widehat{Q}^{y,2p}_{i,j+1/2} - \widehat{Q}^{y,2p}_{i-1/2,j}\right) \leq 0, \tag{6.9}$$

with

$$\begin{aligned}
\widehat{Q}^{x,2p}_{i+1/2,j} &= \widetilde{Q}^{x,2p}_{i+1/2,j} - \frac{1}{2}\overline{\mathbf{v}}^{\top}_{i+1/2,j}\widehat{\mathbf{D}}^x_{i+1/2,j}\langle\!\langle \mathbf{v}\rangle\!\rangle_{i+1/2,j},\\
\widehat{Q}^{y,2p}_{i,j+1/2} &= \widetilde{Q}^{y,2p}_{i,j+1/2} - \frac{1}{2}\overline{\mathbf{v}}^{\top}_{i,j+1/2}\widehat{\mathbf{D}}^y_{i,j+1/2}\langle\!\langle \mathbf{v}\rangle\!\rangle_{i,j+1/2}.
\end{aligned}$$

The proof follows analogously to that of Theorem 4.1.

We term the scheme with fluxes (6.8) as the two-dimensional k-th order TeCNO scheme. It is straightforward to extend the TeCNO schemes to three dimensions on Cartesian meshes.

6.3. **Numerical experiments for two dimensional Euler equations.** We test the TeCNO schemes for the two dimensional Euler equations

$$\begin{aligned}
\rho_t + (\rho u)_x + (\rho v)_y &= 0\\
(\rho u)_t + (\rho u^2 + p)_x + (\rho uv)_y &= 0\\
(\rho v)_t + (\rho uv)_x + (\rho v^2 + p)_y &= 0\\
\mathcal{E}_t + ((\mathcal{E}+p)u)_x + ((\mathcal{E}+p)v)_y &= 0.
\end{aligned} \tag{6.10}$$

Here, the density ρ, velocity field (u,v), pressure p and total energy $\mathcal{E}$ are related by the equation of state

$$\mathcal{E} = \frac{p}{\gamma-1} + \frac{\rho(u^2+v^2)}{2}.$$

The entropy function, fluxes, variables and potentials are given by

$$E(\mathbf{u}) = \frac{-\rho s}{\gamma-1}, \qquad Q^x(\mathbf{u}) = \frac{-\rho u s}{\gamma-1}, \qquad Q^y(\mathbf{u}) = \frac{-\rho v s}{\gamma-1},$$

$$\mathbf{v} = \begin{bmatrix} \frac{\gamma-s}{\gamma-1} - \frac{\rho(u^2+v^2)}{2p} \\ \frac{\rho u}{p}, \frac{\rho v}{p} \\ -\frac{\rho}{p} \end{bmatrix}, \qquad \psi^x(\mathbf{u}) = \rho u, \qquad \psi^y(\mathbf{u}) = \rho v,$$

with s being the thermodynamic entropy.

Defining the parameter vectors

$$\mathbf{z} = \begin{bmatrix} \sqrt{\frac{\rho}{p}} \\ \sqrt{\frac{\rho}{p}}u \\ \sqrt{\frac{\rho}{p}}v \\ \sqrt{\rho p} \end{bmatrix}, \tag{6.11}$$

entropy conservative fluxes for the Euler equations are given by $\widetilde{\mathbf{F}}_{i+1/2} = \begin{bmatrix} \widetilde{\mathbf{F}}^1_{i+1/2} & \widetilde{\mathbf{F}}^2_{i+1/2} & \widetilde{\mathbf{F}}^3_{i+1/2} & \widetilde{\mathbf{F}}^4_{i+1/2} \end{bmatrix}^\top$ and $\widetilde{\mathbf{G}}_{i+1/2} = \begin{bmatrix} \widetilde{\mathbf{G}}^1_{i+1/2} & \widetilde{\mathbf{G}}^2_{i+1/2} & \widetilde{\mathbf{G}}^3_{i+1/2} & \widetilde{\mathbf{G}}^4_{i+1/2} \end{bmatrix}^\top$ with

$$
\begin{aligned}
\widetilde{\mathbf{F}}^1_{i+1/2,j} &= \overline{(z_2)}_{i+1/2,j} (z_4)^{\ln}_{i+1/2,j} \\
\widetilde{\mathbf{F}}^2_{i+1/2,j} &= \frac{\overline{(z_4)}_{i+1/2,j}}{\overline{(z_1)}_{i+1/2,j}} + \frac{\overline{(z_2)}_{i+1/2,j}}{\overline{(z_1)}_{i+1/2,j}} \widetilde{\mathbf{F}}^1_{i+1/2,j} \\
\widetilde{\mathbf{F}}^3_{i+1/2,j} &= \frac{\overline{(z_3)}_{i+1/2,j}}{\overline{(z_1)}_{i+1/2,j}} \widetilde{\mathbf{F}}^1_{i+1/2,j} \\
\widetilde{\mathbf{F}}^4_{i+1/2,j} &= \frac{1}{2\overline{(z_1)}_{i+1/2,j}} \left(\frac{\gamma+1}{\gamma-1} \frac{\widetilde{\mathbf{F}}^1_{i+1/2,j}}{(z_1)^{\ln}_{i+1/2,j}} + \overline{(z_2)}_{i+1/2,j} \widetilde{\mathbf{F}}^2_{i+1/2,j} + \overline{(z_3)}_{i+1/2,j} \widetilde{\mathbf{F}}^3_{i+1/2,j} \right)
\end{aligned}
$$

and

$$
\begin{aligned}
\widetilde{\mathbf{G}}^1_{i,j+1/2} &= \overline{(z_3)}_{i,j+1/2} (z_4)^{\ln}_{i,j+1/2} \\
\widetilde{\mathbf{G}}^2_{i,j+1/2} &= \frac{\overline{(z_2)}_{i,j+1/2}}{\overline{(z_1)}_{i,j+1/2}} \widetilde{\mathbf{G}}^1_{i,j+1/2} \\
\widetilde{\mathbf{G}}^3_{i,j+1/2} &= \frac{\overline{(z_4)}_{i,j+1/2}}{\overline{(z_1)}_{i,j+1/2}} + \frac{\overline{(z_3)}_{i,j+1/2}}{\overline{(z_1)}_{i,j+1/2}} \widetilde{\mathbf{G}}^1_{i,j+1/2} \\
\widetilde{\mathbf{G}}^4_{i,j+1/2} &= \frac{1}{2\overline{(z_1)}_{i,j+1/2}} \left(\frac{\gamma+1}{\gamma-1} \frac{\widetilde{\mathbf{G}}^1_{i,j+1/2}}{(z_1)^{\ln}_{i,j+1/2}} + \overline{(z_2)}_{i,j+1/2} \widetilde{\mathbf{G}}^2_{i,j+1/2} + \overline{(z_3)}_{i,j+1/2} \widetilde{\mathbf{G}}^3_{i,j+1/2} \right).
\end{aligned}
$$

We use Roe-type diffusion matrices Λ^x and Λ^y in the TeCNO diffusion operator.

6.3.1. *Long-time vortex advection.* We start by testing the TeCNO schemes on a smooth test case for the two-dimensional Euler equations, taken from Shu [25]. The initial data is set in terms of velocity u and v, temperature $\theta = \frac{p}{\rho}$ and thermodynamic entropy $s = \log p - \gamma \log \rho$:

$$
u = 1 - (y - y_c)\phi(r), \quad v = 1 + (x - x_c)\phi(r), \quad \theta = 1 - \frac{\gamma - 1}{2\gamma}\phi(r)^2, \quad s = 0,
$$

where (x_c, y_c) is the initial center of the vortex, $r := \sqrt{(x - x_c)^2 + (y - y_c)^2}$ and

$$
\phi(r) := \varepsilon e^{\alpha(1-\tau^2)}, \qquad \tau := \frac{r}{r_c}.
$$

We set the parameters $\varepsilon = \frac{5}{2\pi}$, $\alpha = 1/2$, $r_c = 1$ and $(x_c, y_c) = (5, 5)$. The exact solution to this initial value problem is simply

$$
\mathbf{u}(x, y, t) = \mathbf{u}(x - t, y - t, 0).
$$

In other words, the initial vortex, centered at (x_c, y_c) is advected diagonally with a velocity of 1 in the x- and y-directions.

The computational domain is set to be $[0, 10] \times [0, 10]$ and we use periodic boundary conditions to simulate the flow over the entire plane. We compute up to $t = 100$, During which time the vortex will have traversed through the domain 10 times and should end up exactly where it started. Figure 9 shows the computed density at the final time step on a mesh of 200×200 points. Clearly, there is a significant gain in accuracy with increased order of convergence, and the 3rd and 4th order TeCNO schemes deviate only by a few percent from the exact solution. This experiment illustrates the robust performance of high-order TeCNO schemes in resolving smooth solutions.

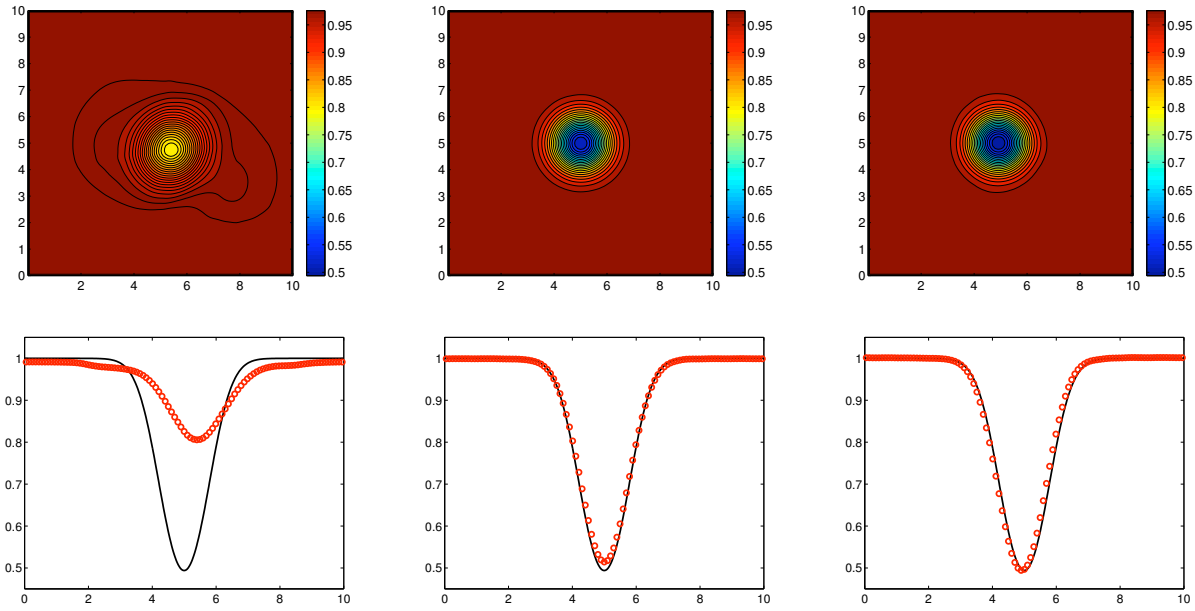

(a) TeCNO2 (b) TeCNO3 (c) TeCNO4

FIGURE 9. TeCNO schemes on the long-time vortex advection problem. Top: ρ at $t = 100$. Bottom: A slice in x-direction at $y = 5$ of TeCNO (circles) and the exact solution (line).

6.3.2. *Vortex-shock interaction.* This problem consists of a single left-moving shock which interacts with a right-moving vortex, and has been taken from [25]. The initial shock has the values

$$\mathbf{u}(x,0) = \begin{cases} \mathbf{u}_L & \text{if } x < 0.5 \\ \mathbf{u}_R & \text{otherwise,} \end{cases}$$

with $(\rho_L, p_L, u_L, v_L) = (1, 1, \sqrt{\gamma}, 0)$ and

$$\rho_R = \rho_L \left(\frac{1 + \beta p_R}{\beta + p_R} \right), \qquad p_R = 1.3$$

$$u_R = \sqrt{\gamma} + \sqrt{2} \left(\frac{1 - p_R}{\sqrt{\gamma - 1 + p(\gamma + 1)}} \right), \qquad v_R = 0.$$

The left state $\mathbf{u}_L$ is then perturbed slightly by adding a vortex. The exact values are specified by the perturbation in velocity, temperature and entropy:

$$\tilde{u} = \frac{y - y_c}{r_c}\phi(r), \quad \tilde{v} = -\frac{x - x_c}{r_c}\phi(r), \quad \tilde{\theta} = -\frac{\gamma - 1}{4\alpha\gamma}\phi(r)^2, \quad \tilde{s} = 0.$$

Here, r and ϕ are exactly as in the previous experiments. We set the free parameters to be $\varepsilon = 0.3$, $(x_c, y_c) = (0.25, 0.5)$, $r_c = 0.05$ and $\alpha = 0.204$. With these parameters, the jump in pressure across the shock wave is about twice as big as the magnitude of the vortex.

We compute on the domain $[0,1] \times [0,1]$ up to time $t = 0.35$. The domain is partitioned into 200×200 grid points. The computed densities are plotted in Figure 10. The results show that the TeCNO schemes resolve both the shock as well as the smooth vortex well. There is a gain in resolution as higher order accurate schemes are employed. The results are comparable to those obtained with standard ENO and WENO schemes in [25].

6.3.3. *Cloud-shock interaction:* The initial data for this test case is set to be

$$\rho = \begin{cases} 3.86859 & \text{if } x < 0.05 \\ 10 & \text{if } r < 0.15 \\ 1 & \text{otherwise} \end{cases} \qquad p = \begin{cases} 167.345 & \text{if } x < 0.05 \\ 10 & \text{otherwise} \end{cases}$$

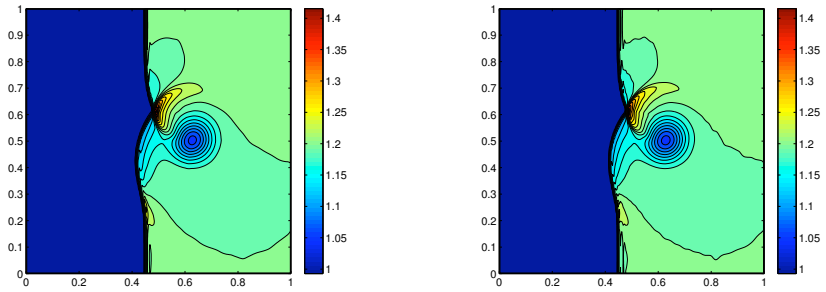

(a) TeCNO2 (b) TeCNO3

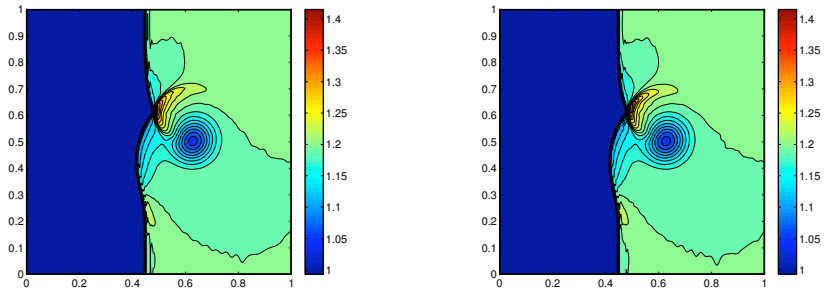

(c) TeCNO4 (d) TeCNO5

FIGURE 10. TeCNO schemes on the shock-vortex interaction problem. The density is plotted at time $t = 0.35$ on a mesh of 200×200 points.

$$u = \begin{cases} 11.2536 & \text{if } x < 0.05 \\ 1 & \text{otherwise} \end{cases} \qquad v \equiv 0.$$

The computational domain is $[0,1] \times [0,1]$ with Neumann type non-reflecting boundary conditions. The exact solution in this case consists of the interaction of a right moving shock with a high density bubble, resulting in a complicated pattern that includes both bow and tail shocks as well as smooth regions in the center of the domain. The computed densities on an mesh of 200×200 points at time $t = 0.06$ are shown in Figure 11. For the sake of comparison, a reference solution computed with the TeCNO3 scheme on a mesh of 1400×1400 points is also shown. The results illustrate that the TeCNO schemes are stable and resolve the complex solution quite well. There is a clear gain in accuracy with the TeCNO3 and TeCNO4 schemes compared to the TeCNO2 scheme.

7. Conclusions

We construct TeCNO finite difference schemes for systems of conservation laws. The schemes do not involve any tuning parameters, and are

(i) arbitrarily high-order accurate for smooth solutions of (1.1).
(ii) entropy stable – they satisfy a discrete entropy inequality (3.11).
(iii) essentially non-oscillatory near discontinuities.

Entropy stability implies that the approximate solutions are bounded in L^p for some p.

The TeCNO schemes combine high-order accurate entropy conservative fluxes with suitable numerical diffusion operators. The high-order entropy conservative fluxes are constructed by taking linear combinations of two-point entropy conservative fluxes. Computationally inexpensive two-point entropy conservative fluxes are described for several well-known conservation laws. Numerical diffusion operators of arbitrary order of accuracy are designed by performing an ENO reconstruction in scaled entropy variables. Entropy stability follows as a consequence of the sign property of the ENO reconstruction, shown in a recent paper [9]. We also prove that the TeCNO schemes converge for linear symmetrizable systems.

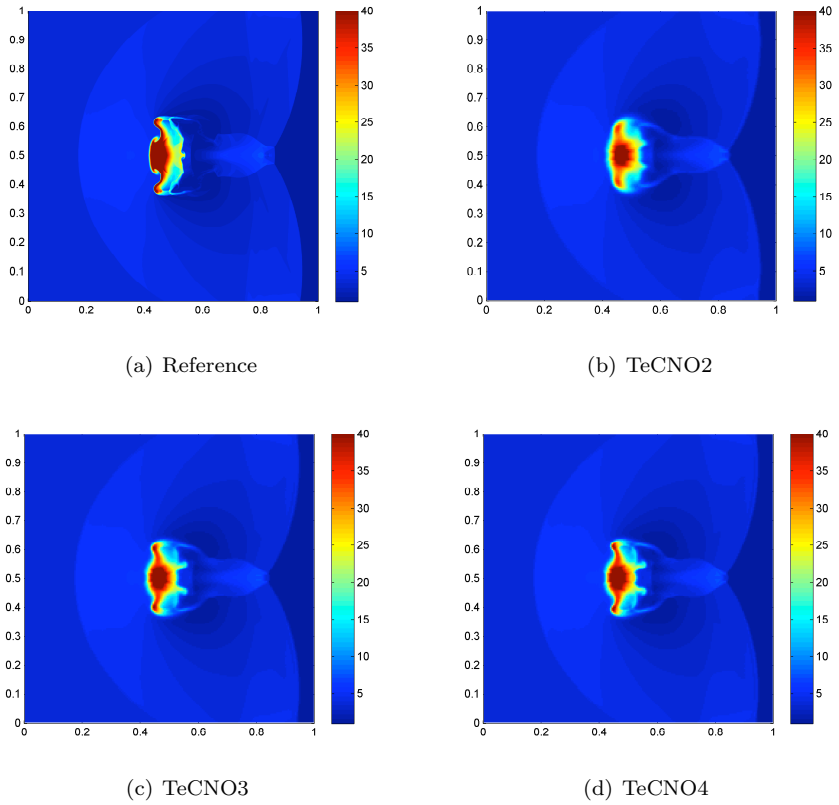

(a) Reference (b) TeCNO2

(c) TeCNO3 (d) TeCNO4

FIGURE 11. TeCNO schemes on the cloud-shock interaction problem. The density at time $t = 0.06$ is plotted on a mesh of 200×200 points. A reference solution is also plotted for comparison.

A large number of numerical examples in one and two space dimensions are presented. They show that the TeCNO schemes are robust. Their numerical performance is comparable to and in some cases superior to standard ENO schemes. The computational cost of TeCNO schemes is also comparable to the ENO schemes with reconstruction in characteristic variables. The main difference between TeCNO schemes and other existing very high order schemes lies in the fact that the TeCNO are rigorously proved to be stable. Hence, we advocate the use of TeCNO schemes on realistic computations of systems of conservation laws.

The extension of TeCNO schemes to several space dimensions require Cartesian meshes. We plan to present TeCNO schemes on unstructured meshes in a forthcoming paper.

REFERENCES

[1] T. J. Barth. Numerical methods for gas-dynamics systems on unstructured meshes. In *An Introduction to Recent Developments in Theory and Numerics of Conservation Laws* pp 195–285. Lecture Notes in Computational Science and Engineering volume 5, Springer, Berlin. Eds: D. Kroner, M. Ohlberger, and Rohde, C., 1999

[2] B. Cockburn, F. Coquel and P. G. LeFloch. Convergence of the finite volume method for multidimensional conservation laws. *SIAM J. Numer. Anal.*, 32 (3), 1995, 687–705.

[3] B. Cockburn and C-W. Shu. TVB Runge-Kutta local projection discontinuous Galerkin finite element method for conservation laws. II. General framework. *Math. Comput.*, 52, 1989, 411–435.

[4] B. Cockburn, S-y. Lin; C-W. Shu. TVB Runge-Kutta local projection discontinuous Galerkin finite element method for conservation laws. III. One-dimensional systems. *J. Comput. Phys.*, 84, 1989, 90–113.

[5] M. G. Crandall and A. Majda. Monotone difference approximations for scalar conservation laws. *Math. Comput.* 34, 1980, 1-21.

[6] C. Dafermos. *Hyperbolic conservation laws in continuum physics.* Springer, Berlin, 2000.

[7] U. S. Fjordholm, S. Mishra and E. Tadmor. Energy preserving and energy stable schemes for the shallow water equations. *"Foundations of Computational Mathematics"*, Proc. FoCM held in Hong Kong 2008 (F. Cucker, A. Pinkus and M. Todd, eds), London Math. Soc. Lecture Notes Ser. 363, pp. 93-139, 2009.

[8] U. S. Fjordholm, S. Mishra and E. Tadmor. Energy stable schemes well-balanced schemes for the shallow water equations with bottom topography. *J. Comput. Phys,* 230, 5587-5609, 2011.
[9] U. S. Fjordholm. S. Mishra and E. Tadmor. ENO reconstruction and ENO interpolation are stable. *Preprint,* 2011.
[10] S. Gottlieb, C. W. Shu and E. Tadmor. High order time discretizations with strong stability properties. *SIAM. Review,* 43, 2001, 89 - 112.
[11] A. Harten. On a class of high-resolution TVD stable finite difference schemes. *SIAM. J. Num. Anal.*, 21, 1984, 1-23.
[12] A. Harten, B. Engquist, S. Osher and S. R. Chakravarty. Uniformly high order accurate essentially non-oscillatory schemes. *J. Comput. Phys.*, 1987, 231-303.
[13] T. J. R Hughes, L. P. Franca and M. Mallet. A new finite element formulation for CFD I: Symmetric forms of the compressible Euler and Navier-Stokes equations and the second law of thermodynamics. *Comp. Meth. Appl. Mech. Eng.*, 54, 1986, 223 - 234.
[14] F. Ismail and P. L. Roe. Affordable, entropy-consistent Euler flux functions II: Entropy production at shocks *Journal of Computational Physics* 228(15), volume 228, 54105436, 2009
[15] G. Jiang and C-W. Shu. Efficient implementation of weighted ENO schemes. *J. Comput. Phys.,* 126, 1996. 202-226.
[16] C. Johnson and A. Szepessy. On the convergence of a finite element method for a nonlinear hyperbolic conservation law. *Math. Comput.*, 49 (180), 1987, 427-444.
[17] B. VanLeer. Towards the ultimate conservative scheme V. A second-order sequel to Godunov's method. *J. Comput. Phys.,* 32, 1979, 101-136.
[18] P. G. LeFloch, J. M. Mercier and C. Rohde. Fully discrete entropy conservative schemes of arbitraty order. *SIAM J. Numer. Anal.,* 40 (5), 2002, 1968-1992.
[19] R. J. LeVeque. Finite volume methods for hyperbolic problems. *Cambridge university press,* Cambridge, 2002.
[20] X-D. Liu and E. Tadmor. Third-order non-oscillatory central scheme for conservation laws. *Numer. Math.*, 79, 1988, 397-425.
[21] H. Nessyahu and E. Tadmor. Non-oscillatory central differencing for hyperbolic conservation laws. *J. Comput. Phys.,* 87, 1990, 408-463.
[22] S. Osher. Riemann solvers, the entropy condition and difference approximations. *SIAM J. Num. Anal.,* 21, 1984, 217-235.
[23] S. Osher and E. Tadmor. On the convergence of difference approximations to scalar conservation laws. *Math. Comput.*, 50, 1988, 19-51.
[24] C. W. Shu and S. Osher. Efficient implementation of essentially non-oscillatory schemes - II, *J. Comput. Phys.*, 83, 1989, 32 - 78.
[25] C. W. Shu. High-order ENO and WENO schemes for Computational fluid dynamics. *In High-order methods for computational physics, T. J. Barth and H. Deconinck eds.,* Lecture notes in computational science and engineering 9, Springer Verlag, 1999, 439-582.
[26] P. Sweby. High resolution schemes using flux limiters for hyperbolic conservation laws. *SIAM J. Num. Anal.*, 21, 1984, 995-1011.
[27] E. Tadmor. Numerical viscosity and entropy conditions for conservative difference schemes. *Math. Comp.*, 43 (168), 369 -381, 1984.
[28] E. Tadmor. The numerical viscosity of entropy stable schemes for systems of conservation laws, I. *Math. Comp.,* 49, 91-103, 1987.
[29] E. Tadmor. Entropy stability theory for difference approximations of nonlinear conservation laws and related time-dependent problems. *Act. Numerica,* 451-512, 2004.
[30] E. Tadmor and W. Zhong. Entropy stable approximations of Navier-Stokes equations with no artificial numerical viscosity. *J. Hyperbolic. Differ, Equ.,* 3 (3), 2006, 529-559.
[31] E. Tadmor and W. Zhong. Energy preserving and stable approximations for the two-dimensional shallow water equations. *In Mathematics and computation: A contemporary view,* Proc. of the third Abel symposium, Ålesund, Norway. Springer, 2008, 67-94.
[32] V. A. Titarev and E. F. Toro. ADER schemes for three-dimensional non-linear hyperbolic systems. *J. Comput. Phys.*, 204(2), 2004, 715-736.

Appendix A. Order of accuracy

Our aim is to show that the scheme with numerical flux (3.8) chosen such that either $2p = k$ for even k or $2p = k + 1$ for odd k, is $(k-1)$-th order accurate. As the entropy conservative fluxes have the desired order of accuracy by the arguments of [18], we need to show that

$$\mathbf{D}_{i+1/2}(\mathbf{v}_{i+1}^- - \mathbf{v}_i^+) - \mathbf{D}_{i-1/2}(\mathbf{v}_i^- - \mathbf{v}_{i-1}^+) = O(\Delta x^k).$$

for (1.6) to be $(k-1)$-th order accurate. We will assume that $\mathbf{D}_{i+1/2}$ is continuous with respect to its two parameters $\mathbf{u}_i, \mathbf{u}_{i+1}$.

For simplicity, we concentrate on the scalar case, denote $v = \mathbf{v}$, and assume for the remainder that $v \in C^k$. Let $p_i^k(x)$ be the interpolant over the point values $v_{i-r_i}, \ldots, v_{i-r_i+k-1}$, with r_i being left shift in cell I_i. By a Taylor expansion, the polynomial approximation has error

$$v(x) - p_i^k(x) = \frac{v^{(k)}(\xi)}{k!} \prod_{m=0}^{k-1} (x - x_{i-r_i+m})$$

for some $\xi \in (x_{i-r}, x_{i-r+k-1})$ dependent on x. Assume for simplicity that the grid is uniform, $x_{i+1} - x_i \equiv \Delta x$. The error at the interface $x_{i+1/2}$ is then

$$v(x_{i+1/2}) - p_i^k(x_{i+1/2}) = \frac{v^{(k)}(\xi_i^+)}{k!} \prod_{m=0}^{k-1} (x_{i+1/2} - x_{i-r_i+m}) = \frac{\Delta x^k v^{(k)}(\xi_i^+)}{k!} \prod_{m=0}^{k-1} (1/2 + r_i - m).$$

Thus, the difference term $\langle\!\langle v \rangle\!\rangle_{i+1/2}$ is

$$\begin{aligned}\langle\!\langle v \rangle\!\rangle_{i+1/2} &= \frac{\Delta x^k}{k!} \left(v^{(k)}(\xi_i^+) \prod_{m=0}^{k-1} (1/2 + r_i - m) - v^{(k)}(\xi_{i+1}^-) \prod_{m=0}^{k-1} (1/2 + r_{i+1} - m) \right) \\ &= \frac{\Delta x^k}{k!} v^{(k)}(\xi_i^+) \left(\prod_{m=0}^{k-1} (1/2 + r_i - m) - \prod_{m=0}^{k-1} (1/2 + r_{i+1} - m) \right) + O(\Delta x^{k+1})\end{aligned}$$

(as $v^{(k)}(\xi_{i+1}^-) - v^{(k)}(\xi_i^+) = O(\Delta x)$). Similarly,

$$\langle\!\langle v \rangle\!\rangle_{i-1/2} = \frac{\Delta x^k}{k!} v^{(k)}(\xi_i^+) \left(\prod_{m=0}^{k-1} (1/2 + r_{i-1} - m) - \prod_{m=0}^{k-1} (1/2 + r_i - m) \right) + O(\Delta x^{k+1}).$$

This proves the claim.

Appendix B. Proof of Theorem 4.3(i)

In this section we prove Theorem 4.3(i), which states that the TeCNO method converges weakly, subsequentially when applied to the system

$$\mathbf{u}_t + \mathbf{A}\mathbf{u}_x = 0, \tag{B.1}$$

for some symmetrizable $\mathbf{A} \in \mathbb{R}^{m \times m}$. Assume for simplicity that $\mathbf{A}$ is symmetric. An entropy/entropy flux pair for (B.1) is then $E(\mathbf{u}) = \frac{1}{2}\mathbf{u}^\top \mathbf{u}$, $Q(\mathbf{u}) = \frac{1}{2}\mathbf{u}^\top \mathbf{A}\mathbf{u}$, with corresponding entropy variables $\mathbf{v}(\mathbf{u}) = E'(\mathbf{u}) = \mathbf{u}$ and entropy potential $\psi(\mathbf{u}) = \frac{1}{2}\mathbf{u}^\top \mathbf{A}\mathbf{u}$. The simplest entropy conservative flux for this entropy is the second-order accurate central scheme (2.9). To this flux we add a diffusion operator to obtain entropy stability. A simple choice would be a Lax-Friedrichs type operator of the form $\mathbf{D}_{i+1/2} = \frac{1}{2}a\mathbf{I}$, where $\mathbf{I}$ is the identity matrix and a is any number $\frac{\Delta x}{2\Delta t} \le a \le \frac{\Delta x}{\Delta t}$. The resulting flux is then

$$\mathbf{F}_{i+1/2} = \frac{1}{2}\mathbf{A}(\mathbf{u}_i + \mathbf{u}_{i+1}) - \frac{a}{2}[\![\mathbf{u}]\!]_{i+1/2}$$

(recall that $\mathbf{v}_i = \mathbf{u}_i$). Higher-order reconstruction of $\mathbf{v} = \mathbf{u}$ would give the flux

$$\mathbf{F}_{i+1/2} = \widetilde{\mathbf{F}}^{2k}_{i+1/2} - \frac{a}{2}\langle\!\langle \mathbf{u} \rangle\!\rangle_{i+1/2}, \tag{B.2}$$

where k is chosen so that $2k \ge p$. We remark that since the diffusion matrix is a constant, diagonal matrix, the ENO-type reconstruction procedure described in Section 3.5 reduce to a standard componentwise ENO reconstruction of $\mathbf{u}$. In particular, each component of the reconstructed values satisfy the sign property (3.17) and the upper jump bound (3.18).

For the remainder, let $\Delta x > 0$ and denote the computed solution by $\mathbf{u}^\Delta(x,t) := \sum_i \mathbf{u}_i(t)\mathbb{1}_{I_i}(x)$.

Lemma B.1. *For all $T > 0$ we have*

$$\|\mathbf{u}^\Delta(T)\|_{L^2(\mathbb{R})} \le \|\mathbf{u}_0\|_{L^2(\mathbb{R})} \tag{B.3}$$

and

$$\int_0^T \sum_i \langle\!\langle \mathbf{u}^\Delta \rangle\!\rangle^2_{i+1/2} \le C. \tag{B.4}$$

Proof. From the proof of Lemma 3.2 one obtains the explicit entropy decay rate

$$\frac{d}{dt}\left(\frac{(\mathbf{u}_i^\Delta)^2}{2}\right) + \frac{1}{\Delta x}\left(\widehat{Q}^{2k}_{i+1/2} - \widehat{Q}^{2k}_{i-1/2}\right) = -\frac{a}{4\Delta x}\left([\![\mathbf{u}^\Delta]\!]^\top_{i+1/2}\langle\!\langle \mathbf{u}^\Delta \rangle\!\rangle_{i+1/2} + [\![\mathbf{u}^\Delta]\!]^\top_{i-1/2}\langle\!\langle \mathbf{u}^\Delta \rangle\!\rangle_{i-1/2}\right),$$

or integrating over $i \in \mathbb{Z}$, $t \in [0,T]$,

$$\|\mathbf{u}^\Delta(T)\|_{L^2}^2 = \|\mathbf{u}^\Delta(0)\|_{L^2}^2 - \frac{a}{2}\int_0^T \sum_i [\![\mathbf{u}^\Delta]\!]_{i+1/2}^\top \langle\!\langle \mathbf{u}^\Delta \rangle\!\rangle_{i+1/2}.$$

By the sign property (3.17), the second term on the right-hand side is nonnegative, which gives (B.3). In particular, because the left-hand side is nonnegative, this second term is bounded from above by $\|\mathbf{u}^\Delta(0)\|_{L^2}^2$. As each component of $\langle\!\langle \mathbf{u}^\Delta \rangle\!\rangle_{i+1/2}$ satisfy the upper bound (3.18), we get (B.4). □

Proof of Theorem 4.3(i). By the L^2 bound (B.3), the sequence $\{\mathbf{u}^\Delta\}$ is uniformly bounded in $L^2\left([0,T], L^2(\mathbb{R})\right)$ by $T\|\mathbf{u}_0\|_{L^2}$. Hence, it converges weakly, subsequentially to some $\mathbf{u} \in L^2\left([0,T], L^2(\mathbb{R})\right)$. We claim that the limit $\mathbf{u}$ is a weak solution of (B.1). Indeed, letting $\phi \in C_0^1(\mathbb{R}\times(0,T))$, multiplying the finite difference scheme by $\phi_i(t) = \phi(x,t)$ and integrating by parts, we get

$$\begin{aligned} 0 &= \int_0^T \Delta x \sum_i \phi_i \frac{d}{dt}\mathbf{u}_i^\Delta + \phi_i \frac{1}{\Delta x}\left(\widetilde{\mathbf{F}}_{i+1/2}^{2k} - \widetilde{\mathbf{F}}_{i-1/2}^{2k}\right) - \phi_i \frac{a}{2\Delta x}\left(\langle\!\langle \mathbf{u}^\Delta \rangle\!\rangle_{i+1/2} - \langle\!\langle \mathbf{u}^\Delta \rangle\!\rangle_{i-1/2}\right) dt \\ &= -\int_0^T \Delta x \sum_i \mathbf{u}_i^\Delta \partial_t \phi_i + \widetilde{\mathbf{F}}_{i+1/2}^{2k} \frac{\phi_{i+1}-\phi_i}{\Delta x} - a\langle\!\langle \mathbf{u}^\Delta \rangle\!\rangle_{i+1/2} \frac{\phi_{i+1}-\phi_i}{\Delta x} dt. \end{aligned}$$

By a standard Lax-Wendroff type argument the first two terms converge to $\int_0^T \int_{\mathbb{R}} \mathbf{u}\phi_t + \mathbf{A}\mathbf{u}\phi_x$, while the third term vanishes:

$$\begin{aligned} \left|\int_0^T \Delta x \sum_{i\in\mathbb{Z}} a\langle\!\langle \mathbf{u}^\Delta \rangle\!\rangle_{i+1/2} \frac{\phi_{i+1}-\phi_i}{\Delta x} dt\right| &\le a\|\phi_x\|_{L^\infty} \left|\int_0^T \Delta x \sum_{i\in S} \langle\!\langle \mathbf{u} \rangle\!\rangle_{i+1/2} dt\right| \\ &\le a\|\phi_x\|_{L^\infty}\sqrt{T}\sqrt{|S|}\Delta x \left(\int_0^T \sum_{i\in S} \langle\!\langle \mathbf{u} \rangle\!\rangle_{i+1/2}^2 dt\right)^{1/2} \le C\sqrt{\Delta x} \to 0 \end{aligned}$$

(where $S = \{i \in \mathbb{Z} : x_i \in \mathrm{supp}(\phi)\}$) by Cauchy-Schwarz and (B.4). □

(Ulrik S.Fjordholm)
ETH Zürich
Seminar for Applied Mathematics
Rämistrasse 101, Zürich, Switzerland.
E-mail address: ulrikf@sam.math.ethz.ch

(Siddhartha Mishra)
ETH Zürich
Seminar for Applied Mathematics
Rämistrasse 101, Zürich, Switzerland.
E-mail address: smishra@sam.math.ethz.ch

(Eitan Tadmor)
Department of Mathematics
Center of Scientific Computation and Mathematical Modeling (CSCAMM)
Institute for Physical sciences and Technology (IPST)
University of Maryland
MD 20742-4015, USA
E-mail address: tadmor@cscamm.umd.edu

Research Reports

No.	Authors/Title
11-39	*U.S. Fjordholm, S. Mishra and E. Tadmor* Arbitrarily high order accurate entropy stable essentially non-oscillatory schemes for systems of conservation laws
11-38	*U.S. Fjordholm, S. Mishra and E. Tadmor* ENO reconstruction and ENO interpolation are stable
11-37	*C.J. Gittelson* Adaptive wavelet methods for elliptic partial differential equations with random operators
11-36	*A. Barth and A. Lang* Milstein approximation for advection–diffusion equations driven by multiplicative noncontinuous martingale noises
11-35	*A. Lang* Almost sure convergence of a Galerkin approximation for SPDEs of Zakai type driven by square integrable martingales
11-34	*F. Müller, D.W. Meyer and P. Jenny* Probabilistic collocation and Lagrangian sampling for tracer transport in randomly heterogeneous porous media
11-33	*R. Bourquin, V. Gradinaru and G.A. Hagedorn* Non-adiabatic transitions near avoided crossings: theory and numerics
11-32	*J. Šukys, S. Mishra and Ch. Schwab* Static load balancing for multi-level Monte Carlo finite volume solvers
11-31	*C.J. Gittelson, J. Könnö, Ch. Schwab and R. Stenberg* The multi-level Monte Carlo Finite Element Method for a stochastic Brinkman problem
11-30	*A. Barth, A. Lang and Ch. Schwab* Multi-level Monte Carlo Finite Element method for parabolic stochastic partial differential equations
11-29	*M. Hansen and Ch. Schwab* Analytic regularity and nonlinear approximation of a class of parametric semilinear elliptic PDEs
11-28	*R. Hiptmair and S. Mao* Stable multilevel splittings of boundary edge element spaces
11-27	*Ph. Grohs* Shearlets and microlocal analysis
11-26	*H. Kumar* Implicit-explicit Runge-Kutta methods for the two-fluid MHD equations